CellPress
Partner Journal

Molecular Plant
Research Article

PDX1.1-dependent biosynthesis of vitamin B_6 protects roots from ammonium-induced oxidative stress

Ying Liu[1,5], Rodolfo A. Maniero[1], Ricardo F.H. Giehl[1], Michael Melzer[2], Priscille Steensma[3], Gabriel Krouk[4], Teresa B. Fitzpatrick[3] and Nicolaus von Wirén[1,*]

[1]Molecular Plant Nutrition, Leibniz Institute of Plant Genetics and Crop Plant Research (IPK), Corrensstrasse 3, 06466 Gatersleben, Germany

[2]Structural Cell Biology, Leibniz Institute of Plant Genetics and Crop Plant Research (IPK), Corrensstrasse 3, 06466 Gatersleben, Germany

[3]Department of Botany and Plant Biology, University of Geneva, 1211 Geneva, Switzerland

[4]BPMP, Université de Montpellier, CNRS, INRA, SupAgro, Montpellier, France

[5]Present address: State Key Laboratory of Crop Genetics and Germplasm Enhancement, College of Resources and Environmental Sciences, Nanjing Agricultural University, Nanjing 210095, China

***Correspondence: Nicolaus von Wirén (vonwiren@ipk-gatersleben.de)**

https://doi.org/10.1016/j.molp.2022.01.012

ABSTRACT

Despite serving as a major inorganic nitrogen source for plants, ammonium causes toxicity at elevated concentrations, inhibiting root elongation early on. While previous studies have shown that ammonium-inhibited root development relates to ammonium uptake and formation of reactive oxygen species (ROS) in roots, it remains unclear about the mechanisms underlying the repression of root growth and how plants cope with this inhibitory effect of ammonium. In this study, we demonstrate that ammonium-induced apoplastic acidification co-localizes with Fe precipitation and hydrogen peroxide (H_2O_2) accumulation along the stele of the elongation and differentiation zone in root tips, indicating Fe-dependent ROS formation. By screening ammonium sensitivity in T-DNA insertion lines of ammonium-responsive genes, we identified *PDX1.1*, which is upregulated by ammonium in the root stele and whose product catalyzes *de novo* biosynthesis of vitamin B_6. Root growth of *pdx1.1* mutants is hypersensitive to ammonium, while chemical complementation or overexpression of *PDX1.1* restores root elongation. This salvage strategy requires non-phosphorylated forms of vitamin B_6 that are able to quench ROS and rescue root growth from ammonium inhibition. Collectively, these results suggest that *PDX1.1*-mediated synthesis of non-phosphorylated B_6 vitamers acts as a primary strategy to protect roots from ammonium-dependent ROS formation.

Key words: ammonium nutrition, apoplastic pH, Fe mobilization, root elongation, pyridoxine, ROS scavenging

Liu Y., Maniero R.A., Giehl R.F.H., Melzer M., Steensma P., Krouk G., Fitzpatrick T.B., and von Wirén N. (2022). PDX1.1-dependent biosynthesis of vitamin B_6 protects roots from ammonium-induced oxidative stress. Mol. Plant. **15**, 820–839.

INTRODUCTION

Nitrogen (N) is an essential mineral element for plant development and is extensively applied in crop production (Xu et al., 2012). While synthetic N fertilizers greatly improve global crop yield, the input of nitrate-based N fertilizers also bears environmental risks when leached as nitrate or emitted as nitrogen oxide (Ju et al., 2009; Sutton et al., 2011). Since ammonium is less prone to leaching than nitrate, ammonium-based N fertilizers are widely used nowadays to replace nitrate in agricultural plant production. To increase fertilizer use efficiency, ammonium is often supplied in locally restricted fertilizer strips, where it is present at very high concentrations (Nkebiwe et al., 2016). Although ammonium is a preferential inorganic N source for many plant species (Gazzarrini et al., 1999), excessive ammonium causes toxicity resulting in leaf chlorosis and suppressed root growth (Britto and Kronzucker, 2002). These symptoms rely on ammonium triggering multiple physiological and morphological responses, including changes in apoplastic and cytosolic pH, gene expression, protein modification, ion transport, N metabolism, redox and phytohormone status, and root system architecture (Britto and Kronzucker, 2002; Li et al., 2014; Liu

Published by the Molecular Plant Shanghai Editorial Office in association with Cell Press, an imprint of Elsevier Inc., on behalf of CSPB and CEMPS, CAS.

and von Wirén, 2017). Against this background and with the increasing use of ammonium-based N fertilizers in agricultural nutrient management, it is important to obtain a deeper understanding of how roots adapt to an ammonium-replete environment.

The most typical morphological changes in root system architecture of ammonium-exposed roots are arrested elongation of primary and lateral roots and enhanced branching of lateral roots (Li et al., 2010; Lima et al., 2010; Liu et al., 2013). Regarding lateral root branching, it has recently been shown that apoplastic acidification caused by AMMONIUM TRANSPORTER (AMT)-mediated ammonium uptake provokes pH-dependent radial auxin diffusion to stimulate locally the emergence of lateral root primordia, forming a highly branched root system (Meier et al., 2020). Given that in several auxin-related mutants root elongation is still as sensitive to ammonium as in wild-type plants, the repression of root elongation by ammonium is unlikely due to altered distribution or action of auxin in plants (Li et al., 2010; Liu et al., 2013). Thus, altered root elongation and lateral root branching under ammonium supply are most likely governed by distinct mechanisms. Neither root elongation nor lateral root branching can be triggered by glutamine, the primary assimilation product of ammonium (Lima et al., 2010; Rogato et al., 2010), suggesting that ammonium itself or ammonium-related metabolites or signals are critical for root development (Liu and von Wirén, 2017). Indeed, excessive ammonium accumulation and hypersensitive root growth of the *cipk23* mutant indicated that ammonium-induced calcium signaling is required to readjust internal NH_4^+/K^+ ratios (Shi et al., 2020). This refers to the function of CIPK23, a CBL-interacting protein kinase, in modulating AMT-, HAK-, and AKT-type transporter activities (Ragel et al., 2015; Straub et al., 2017; Sanchez-Barrena et al., 2020; Dong et al., 2021) with strong impact on cytosolic ammonium accumulation and root growth. A further ammonium-related signal may be ethylene, which appears to modulate genes involved in ammonium uptake and assimilation via the transceptor function of NRT1.1 (Jian et al., 2018). Even though these signaling processes help to maintain cytosolic ammonium homeostasis, they do not explain ammonium-dependent root growth inhibition.

Horizontal split agar experiments indicate that the critical region to sense the inhibitory effect of ammonium on root elongation is the root tip (Li et al., 2010). At the cellular level, both cell division and cell elongation are substantially repressed by ammonium, while the integrity of the root stem cell niche remains unaffected (Liu et al., 2013). In the search for mutants overcoming ammonium-induced root growth inhibition the *vtc1-1* mutant was isolated, which is defective in GMP-mannose pyrophosphorylase (GMPase) and thus not only in downstream ascorbate biosynthesis but also in *N*-glycosylation of proteins (Qin et al., 2008). However, despite its significant impact on ammonium fluxes (Li et al., 2010), GMPase activity turned out not to be the primary cause of ammonium-dependent root growth inhibition (Kempinski et al., 2011). Transcriptome studies have indicated that enhanced formation of reactive oxygen species (ROS) is a typical ammonium-related physiological response (Patterson et al., 2010). Even though significantly higher steady-state H_2O_2 levels in roots were not detected, antioxidative defense systems were induced that comprise ROS-degrading enzymes, including superoxide dismutase (SOD), catalase, peroxidase, guaiacol peroxidase, and glutathione reductase (Patterson et al., 2010). However, in leaves ammonium toxicity increased H_2O_2 formation, which was found to be mediated by ethylene and followed by enhanced peroxidase activity probably via abscisic acid signaling (Li et al., 2019; Sun et al., 2020). Also in the roots of rice, ammonium treatment increased H_2O_2 contents and induced the heme–heme oxygenase *OsSE5* together with other ROS-detoxifying enzymes including SOD, catalase, and ascorbate peroxidase to relieve ammonium-supplied plants from oxidative stress (Xie et al., 2015). These studies indicate that ammonium toxicity causes ROS formation and that the capacity of enzymatic ROS detoxification is a major determinant of ammonium tolerance in plants. So far, evidence for the involvement of non-enzymatic antioxidants in ammonium-induced oxidative stress defense has not been obtained, considering that in roots the pool sizes and oxidative states of NADH, NADPH, glutathione, and ascorbate were not substantially altered by ammonium supply (Patterson et al., 2010).

To explore the mechanisms by which ammonium-exposed roots cope with ammonium toxicity and ammonium-dependent ROS formation, we first used a pharmacological approach unraveling localization of the ammonium-triggered H_2O_2 burst. We then screened mutants of ammonium-responsive genes in roots and identified *PDX1.1*, a gene involved in the biosynthesis *de novo* of vitamin B_6. Chemical complementation and genetic approaches showed that non-phosphorylated forms of vitamin B_6 suppressed H_2O_2 formation under ammonium supply. With PDX1.1-dependent vitamin B_6 formation, our study identifies a protective mechanism that spatially overlaps with ammonium-triggered H_2O_2 formation in inner root cells and thus carries potential to better adapt plant roots to ammonium-based fertilization strategies.

RESULTS

Accumulation of H_2O_2 under ammonium supply inhibits primary root elongation

When wild-type seedlings of *Arabidopsis* were grown on half-strength Murashige and Skoog (MS) medium for 6 days in the presence of either 1 or 10 mM ammonium as the sole N source, primary root length became 25% or 35% shorter, respectively, than that of nitrate-grown plants (Supplemental Figure 1A and 1B). Likewise, total and mean length of lateral roots were repressed to a similar extent as primary root length, suggesting a common mechanism underlying ammonium-induced growth inhibition in both root types (Supplemental Figure 1B–1D). A significant dose-dependent decrease in root elongation rate already set in after 1 day of ammonium exposure, suggesting a rapid inhibitory mechanism (Supplemental Figure 1E–1G). Root exposure to ammonium decreased both cortical cell length and meristem size in a dose-dependent manner and to a similar extent (Supplemental Figure 1H–1J). Since cytokinins determine root meristem size by controlling cell differentiation (Dello Ioio et al., 2007), we checked the response of cytokinin-sensitive reporter line *TCS:GFP* in the primary root apex, which showed highest expression in the columella and lateral root cap and slight but significant repression

under ammonium, revealing that cytokinin signaling was not enhanced by ammonium (Bielach et al., 2012; Supplemental Figure 2A and 2B). The histidine kinase AHK3 acts as a cytokinin receptor to stimulate a two-component signaling pathway that transfers a phosphorelay signal to the nucleus, where transcription factors of the type-B ARABIDOPSIS RESPONSE REGULATOR gene family (ARR-B) are activated (Ferreira and Kieber, 2005). We therefore examined ammonium sensitivity by measuring primary root length and meristem size in the *ahk3-3*, *arr1-3*, and *arr12-1* mutants, which however revealed no difference from the wild type (Supplemental Figure 2C–2F), indicating that the AHK3/ARR1 and AHK3/ARR12 two-component cytokinin signaling pathway was not targeted by ammonium. SHY/IAA3 acts directly downstream of ARR1 and ARR12, which increases cell differentiation rate and balances root meristem size at the transition zone (Dello Ioio et al., 2008). However, neither the *SHY2* deletion line *shy2-31* nor *shy2-2*, which expresses a stabilized proteoform of SHY2 (Tian et al., 2002), exhibited altered ammonium sensitivity of primary root elongation or meristem formation (Supplemental Figure 2G–2J). Taken together, these observations indicated that cytokinin signaling is not involved in ammonium-dependent inhibition of root elongation.

As ammonium has been reported to enhance ROS levels in plants (Patterson et al., 2010; Xie et al., 2015), we stained H_2O_2 in primary roots by 3,3′-diaminobenzidine (DAB). Compared with nitrate, increasing ammonium supply gradually enhanced repression of cell length and meristem size with the detection of H_2O_2, particularly in the elongation and differentiation zones of the root apex (Figure 1A–1G). Since nitrate-supplied plants also showed DAB staining similar to that in ammonium-exposed plants in the meristematic root zone, this zone was not considered as a primary target of ammonium-induced ROS production. To better understand the source of ammonium-dependent ROS formation in primary roots, we employed a pharmacological approach and first applied potassium iodide (KI), acting as a chemical H_2O_2 scavenger (Lee et al., 2013). KI largely reversed the ammonium-dependent inhibition of the primary root elongation rate and restored cell length and meristem size to a large extent (Figure 1A–1F). Recovered root elongation coincided with lower abundance of DAB-stained ROS in the elongation and differentiation zone of the primary root (Figure 1G), suggesting that enhanced levels of H_2O_2 are responsible for the stunted root phenotype. When ammonium-grown roots were exposed to elevated H_2O_2 levels, which were generated either directly by supply of 1 mM H_2O_2 or indirectly by supply of the peroxidase inhibitor salicylhydroxamic acid (SHAM), primary root elongation rates declined drastically due to strongly decreased cell length and meristem size, consistent with enhanced DAB staining (Supplemental Figure 3A–3G). Notably, in nitrate-supplied roots, meristem size and DAB staining were apparently not affected by H_2O_2 or SHAM while cortical cell length was only slightly decreased (Supplemental Figure 3D–3G), relating to the fact that nitrate-supplied plants possess elevated ROS-scavenging capacities (Chu et al., 2021). To distinguish between the contribution of superoxide radicals ($O_2^{\bullet-}$) and H_2O_2, we investigated the effects of sodium diethyldithiocarbamate (DDC), an inhibitor of Cu,Zn-SOD that blocks H_2O_2 generation and leads to $O_2^{\bullet-}$ accumulation (Auh and Murphy, 1995). Both cell length and meristem size of the primary root apex were partially but significantly rescued by DDC supplementation, allowing partial recovery of primary root elongation (Supplemental Figure 4). This observation indicated that $O_2^{\bullet-}$ radicals are not the direct cause of ammonium-mediated inhibition of root elongation, whereas SOD-catalyzed conversion of $O_2^{\bullet-}$ to H_2O_2 matters. Alternatively, we suspected that respiratory burst oxidase homolog (RBOH)-type NADPH oxidases produce ammonium-dependent ROS and examined a few *rboh* single or multiple knockout lines. However, none of them showed an ammonium-dependent root phenotype (Supplemental Figure 5).

Since in the absence of ammonium H_2O_2 was less effective in inhibiting root elongation (Supplemental Figure 3), we assumed that ammonium-facilitated formation of H_2O_2 plays a role and speculated that this process depends on the availability of iron (Fe) (Dixon and Stockwell, 2014). Indeed, lowering Fe supply from 100 μM to 10 μM Fe(III)-EDTA resulted in weaker inhibition of cell length, meristem size, and primary root elongation and prevented accumulation of DAB-stained ROS in the elongation and differentiation zone of the primary root (Figure 1A–1G). Higher resolution of DAB-stained cells allowed assignment of H_2O_2 to the stele of the late elongation and early differentiation zone, which became shorter under increasing ammonium supply and thus appeared more apical (Figure 2A). In addition, we localized ROS-dependent fluorescence by the cell-permeant indicator 2′,7′-dichlorofluorescin diacetate (H_2DCFDA), revealing enhanced ROS formation in the stele, especially along the vascular strands of ammonium-exposed roots with a maximum at the transition of the elongation to the differentiation zone (Figure 2B and 2C). Considering Fe dependency of ammonium-triggered root inhibition (Figure 1), Fe distribution in the root was stained by DAB-enhanced Perls detecting both free Fe(II) and Fe(III) (Roschzttardtz et al., 2009). While nitrate-grown roots accumulated some Fe in the meristematic zone, ammonium-exposed roots showed much higher Fe accumulation, especially in the differentiation zone (Figure 2D). Cross-sections of Perls/DAB-stained primary roots showed that ammonium-dependent Fe precipitation was restricted by the Casparian band and thus confined to the apoplast of outer root cells (Supplemental Figure 6). Since Fe availability increases with decreasing pH and ammonium nutrition is known to acidify the rhizosphere and apoplast (Romheld and Marschner, 1986; Meier et al., 2020), apoplastic pH changes were traced by using the apopHusion line, a ratiometric reporter of apoplastic pH (Gjetting et al., 2012). Increasing ammonium nutrition decreased apoplastic pH, particularly in the elongation and differentiation zone of ammonium-exposed roots (Figure 2E and 2F), which co-localized with DAB- or fluorescence-stained ROS (Figure 2A–2D), suggesting that the ammonium-dependent pH decrease and enhanced Fe availability caused ROS formation.

Since ammonium-induced repression of root elongation appears to be a rapid response detected even 1 day after ammonium exposure (Supplemental Figure 1E–1G), we investigated dynamic changes in Fe availability and ROS status in ammonium-supplied primary roots. Enhanced Fe precipitation and ROS accumulation appeared as early as 1 day after ammonium supply in the differentiation zone of the primary root and progressed in the apical direction with time and in dependence of external ammonium supply (Supplemental Figure 7). As indicated by the arrows marking the boundaries of the meristematic and elongation zones, the size of the elongation zone started declining earlier than that of the meristematic

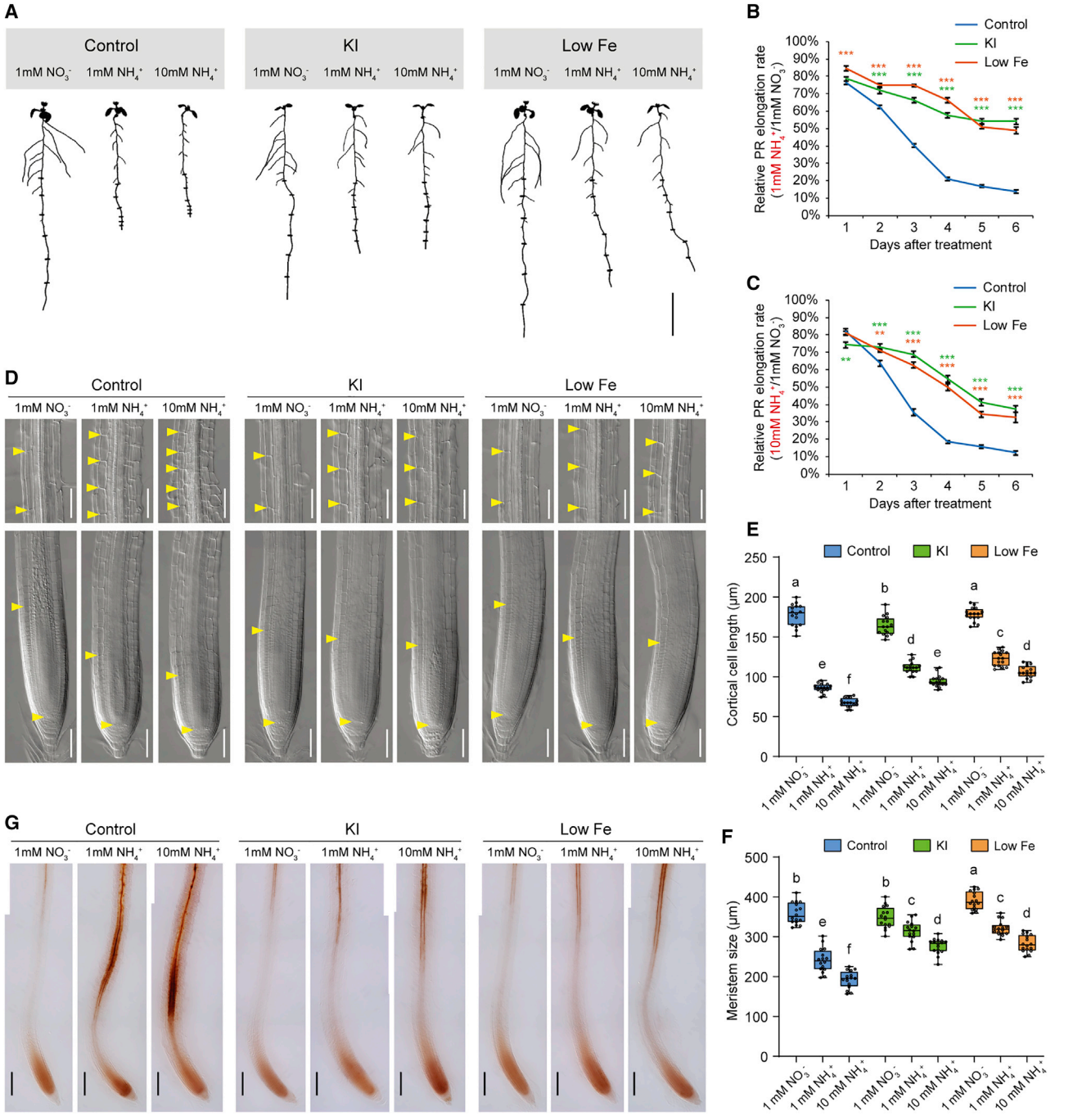

Figure 1. Involvement of H_2O_2 and Fe in ammonium-dependent root growth inhibition.

(A) Root phenotype of wild-type plants 6 days after transfer to different N supply, which contained additionally either 0.5 mM KI or 10 μM Fe(III)-EDTA (low Fe) instead of 100 μM Fe(III)-EDTA as in control plates. Horizontal marks along the root axis indicate daily positions of primary root tips. Root images were scanned 6 days after transfer. Scale bar, 1 cm.

(B and C) Relative primary root elongation rate under 1 mM ammonium supply **(B)** or under 10 mM ammonium supply **(C)**, normalized to the growth rate of plants treated with 1 mM nitrate. Symbols represent means ± SE, $n = 20$ plants per treatment. Asterisks denote significant differences between control and indicated treatments at each time point as $^*P < 0.05$ $^{**}P < 0.01$, $^{***}P < 0.001$ according to Dunnett's multiple test.

(D) Cell length and meristem size of primary roots. The length of mature cortical cells and the size of the root apical meristem are indicated by yellow arrowheads. DIC images of primary root tips were taken at 6 days after transfer. Scale bars, 100 μm.

(E and F) Quantitative readout of mature cortical cell length **(E)** and primary root meristem size **(F)**. Boxes show the first quartile, median, and third quartile; whiskers show the minimum and maximum values, $n = 16$ plants. Different letters represent significant differences between treatments according to two-way ANOVA followed by Tukey's HSD test, $P < 0.05$.

(G) DAB staining of H_2O_2 in primary root tips at 6 days after treatment. The reddish-brown coloration indicates H_2O_2. Representative images from 10 plants per treatment are shown. Scale bars, 200 μm.

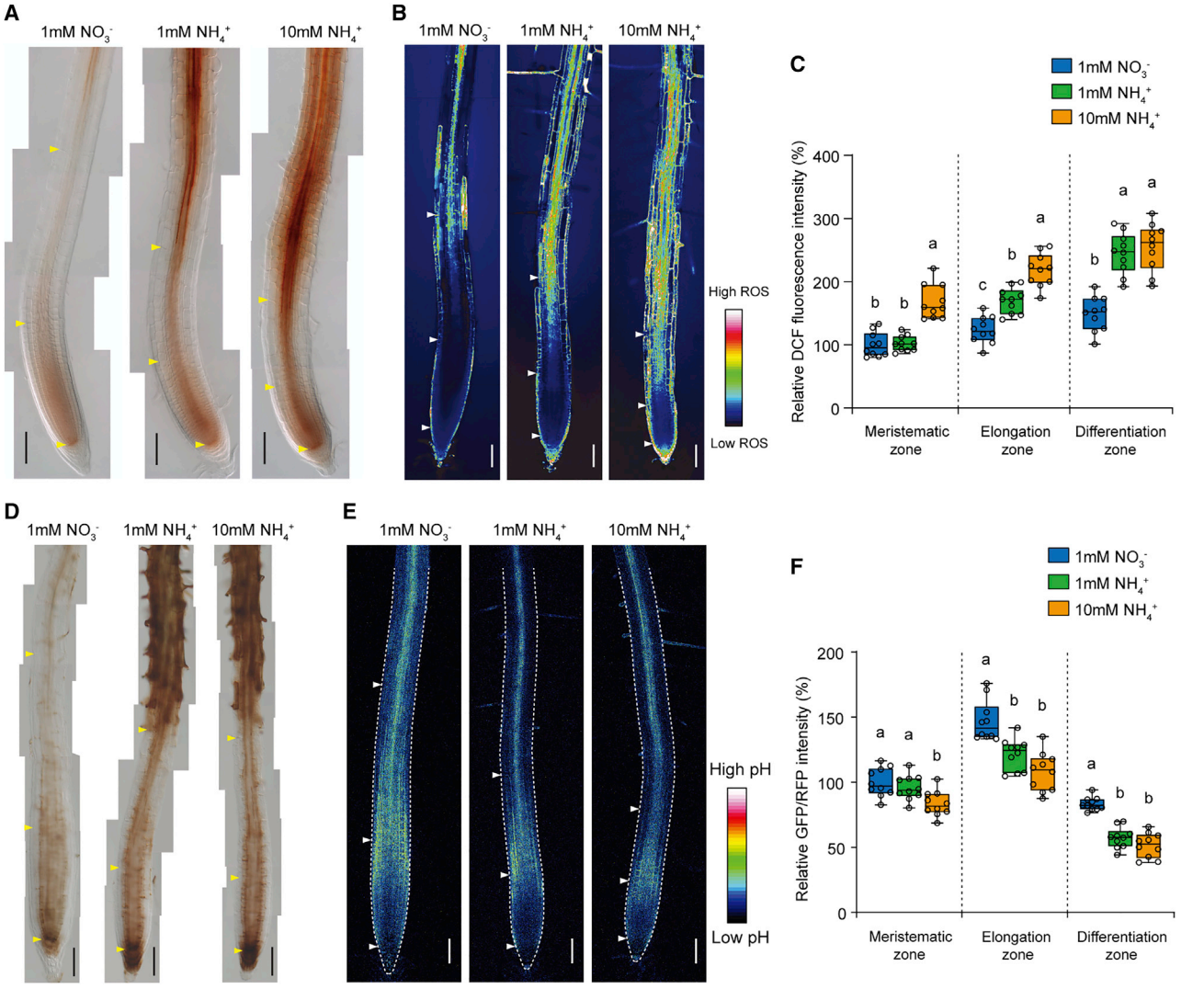

Figure 2. Ammonium-dependent histochemical changes in the primary root apex.

(A) DAB staining of H_2O_2 in primary root tips at 6 days after treatment. The reddish-brown coloration indicates H_2O_2. Representative images from 10 plants per treatment are shown. Scale bars, 100 μm.

(B) Staining of ROS (oxidant levels) by H_2DCFDA staining. Rainbow color code (black to white) indicates DCF fluorescence intensity (low to high). Scale bars, 100 μm.

(C) Quantitative readout of the fluorescence intensity of H_2DCFDA staining in different zones of the primary root. The boxes show the first quartile, median, and third quartile; whiskers show the minimum and maximum values, $n = 10$ independent plants. Different letters represent significant differences within each individual root zone at $P < 0.05$ according to Tukey's HSD test.

(D) Perls/DAB staining of Fe as indicated by a reddish-brown color. Scale bars, 100 μm.

(E) Activity of the apoplastic pH sensor apo-pHusion. Color code (black to white) indicates fluorescence intensity ratio of eGFP/mRFP1 (low to high) and thus apoplastic pH. Scale bars, 100 μm.

(F) Quantitative readout of the intensity ratio of eGFP/mRFP in different developmental zones of the primary root. Boxes show the first quartile, median, and third quartile; whiskers show the minimum and maximum values, $n = 10$ independent plants. Different letters represent significant differences within each individual root zone at $P < 0.05$ according to Tukey's HSD test. After a pre-culture of 6 days, wild-type or apo-pHusion plants were transferred to the treatment medium supplied with differing N forms. Histological staining and fluorescent imaging were performed 6 days after treatment. Representative images from 10 plants per treatment are shown. Yellow arrowheads in **(A)** and **(D)**, or white arrowheads in **(B)** and **(E)**, indicate the boundaries of the meristematic zone, elongation zone, and differentiation zone along the primary root.

zone, consistent with progression of H_2DCFDA-dependent fluorescence into the elongation zone toward the meristematic zone (Figure 2B and Supplemental Figure 7B). To verify an impact of ROS on cell division, we evaluated the response to ammonium of the cell-cycle reporter *CycB1;1::GUS* (Colón-Carmona et al., 1999). Ammonium supply significantly suppressed β-glucuronidase (GUS) activity in the apical meristem of primary root, and this suppression was largely alleviated by lowering the external Fe supply (Supplemental Figure 8). Consistent with the decrease of meristem size and cell length under the same conditions (Figure 1D–1F), we conclude that Fe-dependent ROS formation is a major repressor

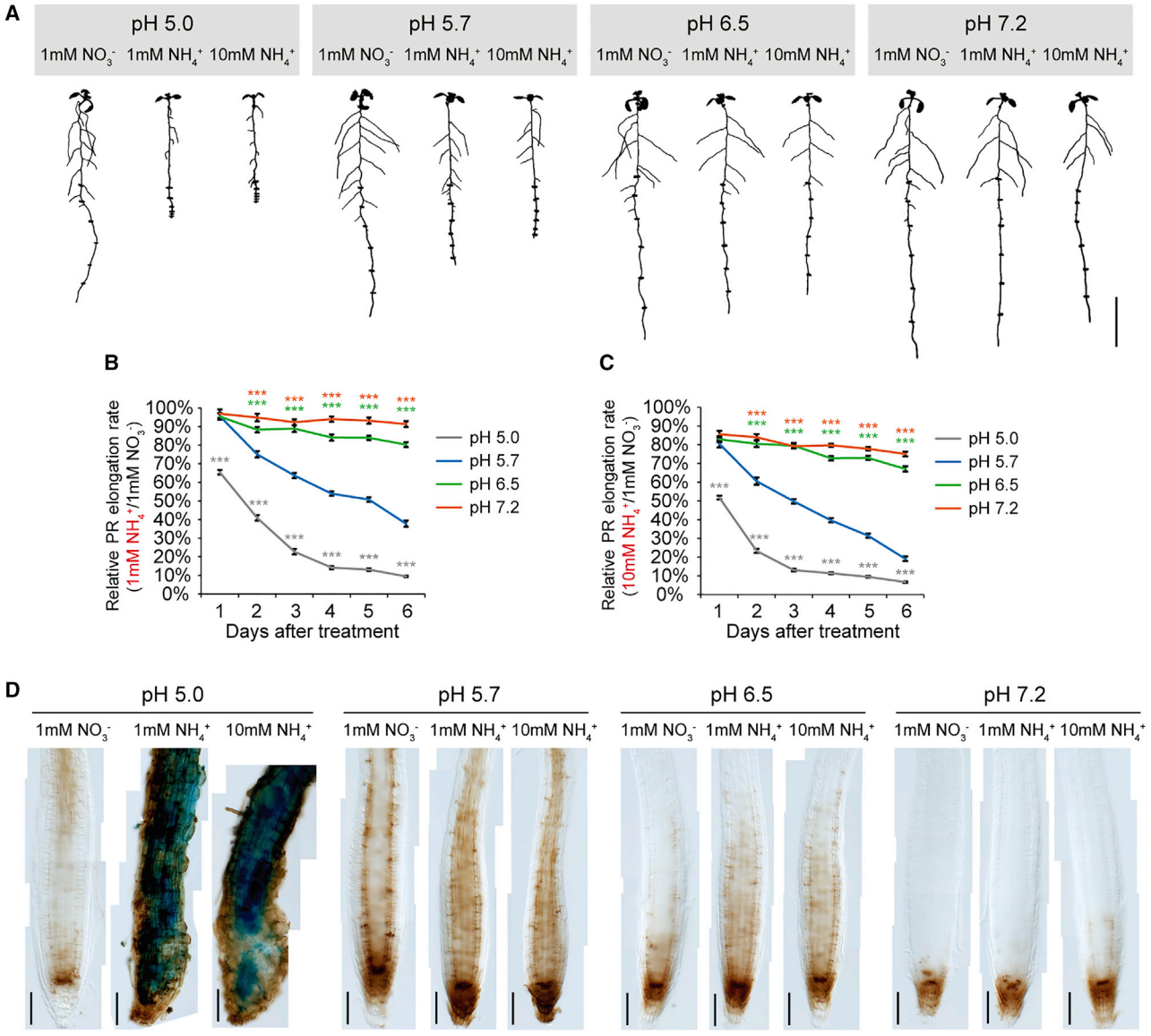

Figure 3. Influence of medium pH on primary root growth and Fe accumulation in roots.

(A) Root phenotype of wild-type plants 6 days after transfer to different N supply buffered at different pH. Medium pH of 5.0, 5.7, and 6.5 was buffered by 2.5 mM MES, while pH 7.2 was buffered by 2.5 mM MOPS. Horizontal marks along the root axis indicate daily positions of primary root tips. Scale bar, 1 cm.

(B and C) Relative primary root elongation rate under 1 mM ammonium supply **(B)** or under 10 mM ammonium supply **(C)**, normalized to the growth rate of plants treated with 1 mM nitrate. Symbols represent means ± SE, $n = 20$ plants per treatment. Asterisks denote significant differences between control (pH 5.7) and indicated treatments at each time point as $^{*}P < 0.05$, $^{**}P < 0.01$, $^{***}P < 0.001$ according to Dunnett's multiple test.

(D) Perls/DAB staining of Fe as indicated by a reddish-brown color. Perls/DAB staining was conducted at 6 days after transfer. Representative images from 10 plants per treatment are shown. Scale bars, 100 μm.

of both cell elongation and cell division in ammonium-exposed root apices. Notably, exactly the same responses of apoplastic pH, Fe availability, and ROS formation as in primary root were detected in the apex of lateral roots (Supplemental Figure 9), indicating that oxidative stress acts as a common inhibitory mechanism underlying ammonium-induced growth repression in both primary and lateral roots.

To manipulate Fe availability in the presence of ammonium, we buffered medium pH at different values (Supplemental Figure 10). While ammonium-inhibited root elongation was aggravated when roots were shifted from standard pH 5.7 to pH 5.0, higher pH restored root elongation, leading to almost similar length of nitrate- and ammonium-grown roots at pH 7.2 (Figure 3A–3C). After 6 days of ammonium exposure, Perls/DAB staining revealed decreasing Fe accumulation in the apical root zone with increasing pH, except for the columella cells (Figure 3D). In contrast, strongly enhanced amounts of Fe accumulated at pH 5.0 but only in ammonium-exposed roots. Since the pH of the agar medium was buffered by 2-*(N-morpholino)ethanesulfonic acid* (MES), we suspected that buffer strength might affect ammonium-induced pH changes and Fe

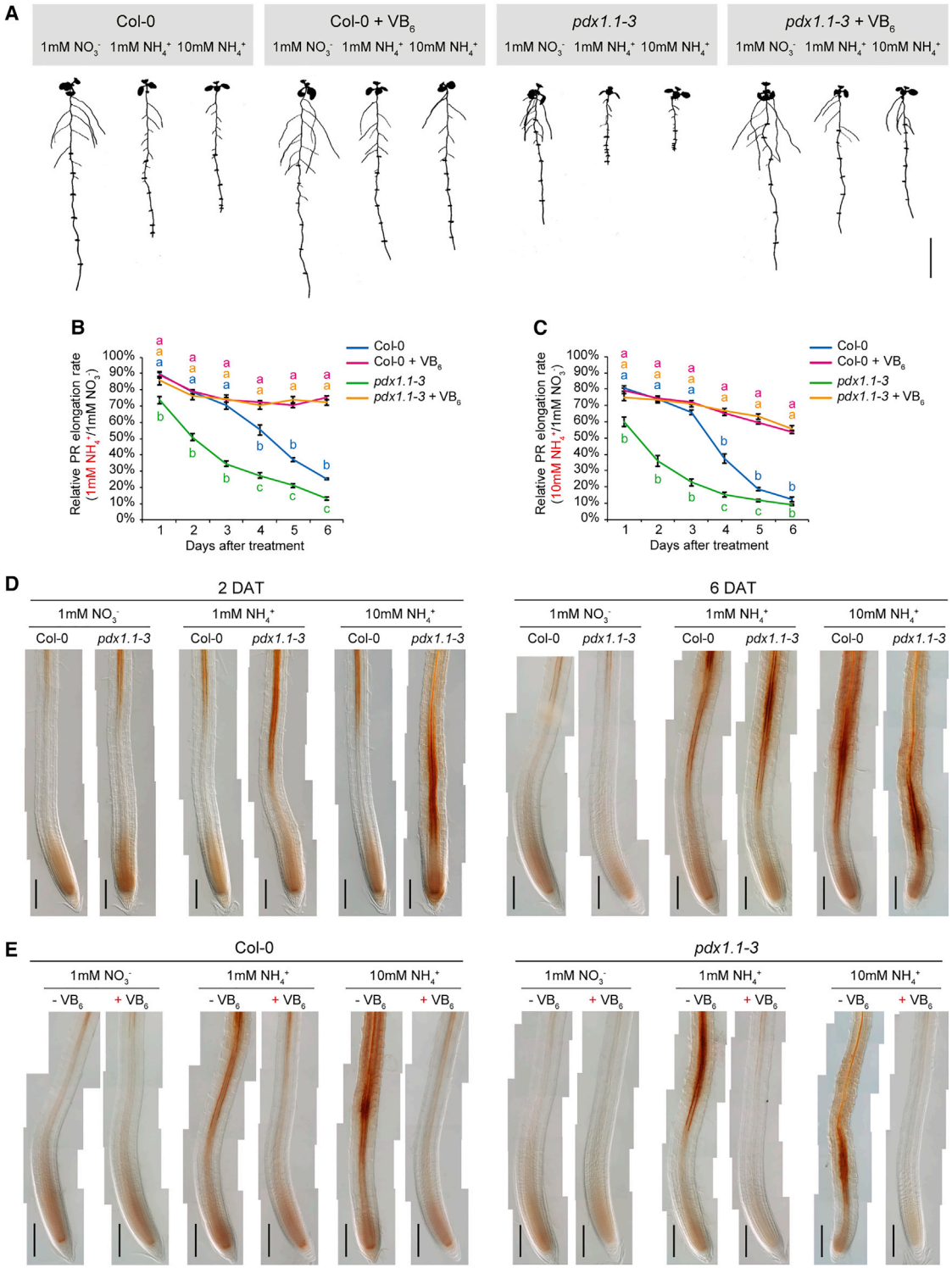

Figure 4. Exogenous application of vitamin B_6 alleviates ammonium toxicity in roots.

(A) Root phenotype of Col-0 and *pdx1.1-3* mutant plants 6 days after transfer to different N supply in the absence or presence of 5 μM vitamin B_6 (pyridoxine). Horizontal marks along the root axis indicate daily positions of primary root tips. Scale bar, 1 cm.

(B and C) Relative primary root elongation rate under 1 mM ammonium supply **(B)** or under 10 mM ammonium supply **(C)**, normalized to the growth rate of plants treated with 1 mM nitrate. Data represent means ± SE, $n = 20$ plants per treatment. Different letters represent significant differences at each time point at $P < 0.05$ according to Tukey's HSD test.

(legend continued on next page)

availability under ammonium supply. Indeed, lowering MES concentration from 2.5 to 0.5 mM dramatically aggravated Fe precipitation and inhibition of ammonium-exposed primary root tips, while at 10 mM MES Fe precipitation decreased and ammonium-repressed root elongation was partially attenuated (Supplemental Figure 11). These results indicated that the intensity of ammonium-dependent proton release and acidification of the rhizosphere is of immediate relevance for Fe mobilization and precipitation in the root apoplast and at the root surface.

The dependence of ammonium-induced root growth inhibition on Fe recalls the role of Fe in root growth inhibition under phosphate deficiency that also relies on Fe-facilitated ROS formation (Müller et al., 2015). Recently, it has been reported that this role of Fe represents a side effect of light exposure when roots are grown in transparent Petri dishes (Zheng et al., 2019). Thus, we shaded the whole root system by aluminum foil as described by Zheng et al. (2019) and noted that in all N treatments primary root length increased when roots were shaded from white light (Supplemental Figure 12A and 12B). Even though ammonium-dependent primary root growth inhibition was slightly alleviated by shielding roots from light, ammonium supply still arrested primary root elongation to a large extent (Supplemental Figure 12B and 12C). This observation supported that light increases the pool of redox-active Fe (Zheng et al., 2019), which in the presence of ammonium may engage in ROS formation and inhibit primary root elongation.

Previous work under phosphate deficiency showed that blue light exposure promotes the Fenton reaction converting H_2O_2 to hydroxyl radicals that are more toxic oxygen species and strongly suppress primary root elongation (Zheng et al., 2019). Here, to evaluate the involvement of hydroxyl radicals in ammonium-dependent root growth inhibition, we supplied thiourea, a chemical scavenger of hydroxyl radicals (Wasil et al., 1987), together with ammonium to the medium. However, the presence of thiourea hardly altered the sensitivity of primary roots to ammonium (Supplemental Figure 13), indicating that the formation of hydroxyl radicals via the Fenton reaction is not critical for ammonium-dependent root growth inhibition.

Hypersensitivity of root elongation to ammonium relates to vitamin B_6 deficiency

To explore how plants cope with ammonium-induced H_2O_2 formation and subsequent root growth inhibition, we searched publicly available transcriptome data for ammonium-responsive genes that are expressed in roots (Patterson et al., 2010; Ristova et al., 2016). We then collected T-DNA insertion lines of 29 ammonium-responsive genes and screened them for primary root length under ammonium versus nitrate supply (Supplemental Data 1). In this screen, we identified a T-DNA insertion line of *PDX1.1* (*SALK_024245*), which was hypersensitive to ammonium treatment (Supplemental Figure 14A and 14B). In *Arabidopsis*, PDX1.1 (along with PDX2) catalyzes vitamin B_6 biosynthesis *de novo* (Tambasco-Studart et al., 2005; Supplemental Figure 15); thus, *pdx1.1* mutants suffer from vitamin B_6 deficiency (Titiz et al., 2006; Wagner et al., 2006; Boycheva et al., 2015). We confirmed the hypersensitive phenotype of *pdx1.1* mutants to ammonium by examining primary root growth in *SALK_024245* and the transposon insertion line *pdx1.1-1* (Supplemental Figure 14C–14E). Since *SALK_024245* and *pdx1.1-1* showed the same growth phenotype under ammonium supply in all our experiments, we focused in the following on *SALK_024245*, naming it *pdx1.1-3*. Given that under nitrate supply primary root growth of *pdx1.1-3* was weaker (Figure 4A), we calculated the relative primary root elongation rate by normalizing it to the root growth rate under nitrate. An earlier and steeper decrease in root elongation rate of *pdx1.1-3* than of the wild type confirmed hypersensitivity of *pdx1.1-3* to ammonium nutrition (Figure 4B and 4C). The higher sensitivity of *pdx1.1-3* to ammonium accompanied elevated accumulation of H_2O_2 in ammonium-exposed primary root tips as soon as 2 days after transfer to ammonium (Figure 4D).

To confirm whether the hypersensitivity of *pdx1.1-3* to ammonium is due to the defect in vitamin B_6 biosynthesis, we supplied vitamin B_6 in the form of pyridoxine to the growth medium. While external supply of pyridoxine to nitrate-grown wild-type plants had no effect, it largely alleviated ammonium-induced inhibition of primary root growth in the wild type and particularly in the *pdx1.1-3* mutant (Figure 4A). Notably, external supplementation of pyridoxine recovered completely the primary root elongation rate of *pdx1.1-3* (Figure 4B and 4C), cortical cell length, and meristem size (Supplemental Figure 16) as well as GUS activity of the *CycB1;1::GUS* reporter (Supplemental Figure 17), confirming that the hypersensitive phenotype of *pdx1.1-3* to ammonium is due to defective vitamin B_6 biosynthesis. Since external supply of pyridoxine reduced also the accumulation of DAB-stained H_2O_2 in ammonium-treated primary roots of both lines (Figure 4E), we conclude that vitamin B_6 alleviates ammonium toxicity either by suppressing H_2O_2 generation or by scavenging H_2O_2 in primary root tips.

Non-phosphorylated forms of vitamin B_6 are critical for ammonium detoxification

Vitamin B_6 is essential for all living organisms, and refers to a group of six different vitamers that contain a pyridine ring and include the non-phosphorylated forms pyridoxal (PL), pyridoxine (PN), and pyridoxamine (PM), as well as the phosphorylated forms pyridoxal 5′-phosphate (PLP), pyridoxine 5′-phosphate (PNP), and pyridoxamine 5′-phosphate (PMP) (Fitzpatrick, 2011; Supplemental Figure 15). To evaluate their efficacy in mitigating root growth inhibition, we supplied different B_6 vitamers to the medium. Compared with the mock treatment, external supply of PLP slightly retarded the ceasing primary root elongation during the first 4 days after transfer to ammonium, but it scarcely restored primary root length after 6 days of ammonium supply

(D) H_2O_2 accumulation in the primary root as visualized by DAB staining in wild-type and *pdx1.1-3* mutant plants under differing N supply. DAB staining was conducted 2 days after treatment (2DAT) or 6 days after treatment (6DAT). Representative images from 10 seedlings per treatment are shown. Scale bars, 200 μm.

(E) DAB staining of H_2O_2 in primary root tips 6 days after treatment. The reddish-brown coloration indicates H_2O_2. Representative images from 10 seedlings per treatment are shown. Scale bars, 200 μm.

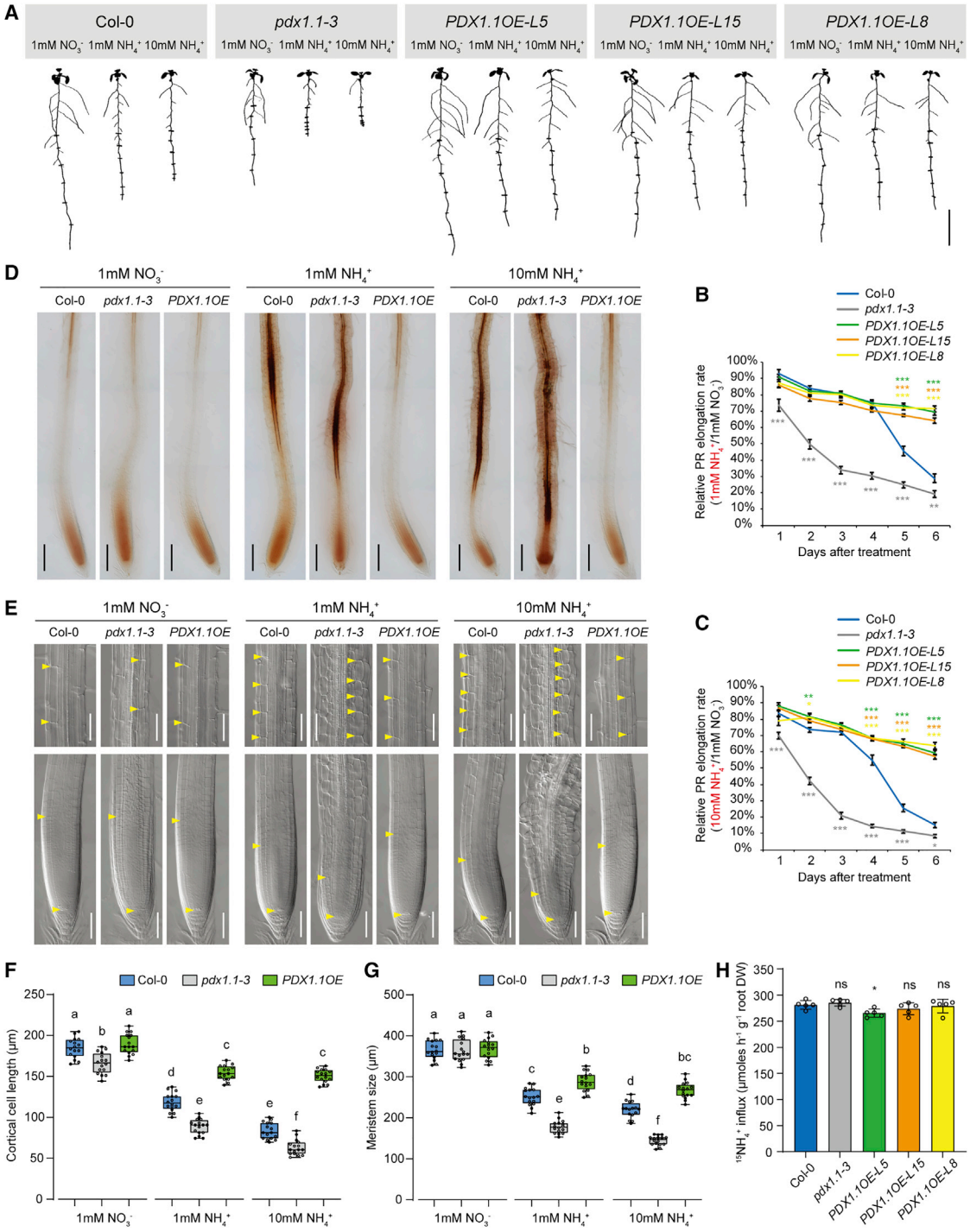

Figure 5. Overexpression of *PDX1.1* enhances ammonium tolerance in roots.

(A) Root phenotype of wild-type, *pdx1.1-3* mutant, and three independent *PDX1.1* overexpression lines subjected to different N supply. Horizontal marks along the root axis indicate daily positions of primary root tips. After pre-culture of 6 days, plants were transferred to media containing different N forms. Root images were taken at 6 days after transfer. Scale bar, 1 cm.

(B and C) Relative primary root elongation rate under 1 mM ammonium supply **(B)** or under 10 mM ammonium supply **(C)**, normalized to the growth rate of plants treated with 1 mM nitrate. Symbols represent means ± SE, $n = 20$ plants per treatment. Asterisks denote significant differences between wild type and indicated lines at each time point as $^{*}P < 0.05$, $^{**}P < 0.01$, $^{***}P < 0.001$ by Dunnett's multiple test.

(D) DAB staining of H_2O_2 in primary root tips of wild type, *pdx1.1-3*, and *PDX1.1OE-L5* at 6 days after treatment. The reddish-brown coloration indicates H_2O_2. Representative images from 10 plants per treatment are shown. Scale bars, 200 μm.

(legend continued on next page)

(Supplemental Figure 18A–18C). By contrast, exogenous application of the vitamin B_6 forms PL or PN effectively rescued primary root growth under ammonium supply even during later stages of the treatment, indicating a superior efficacy of the non-phosphorylated B_6 vitamers. When monitoring the H_2O_2 status in root tips in parallel with root elongation, exogenous application of PN or PL but not of PLP quenched excess accumulation of H_2O_2 in ammonium-treated primary root tips (Supplemental Figure 18D). These results reveal that mitigation of root growth inhibition refers to the non-phosphorylated forms of vitamin B_6 and their ability to suppress H_2O_2 accumulation.

Overexpression of *PDX1.1* improves ammonium tolerance in roots

To address the question of whether PDX1.1 plays a role in eliminating ammonium-triggered ROS, we inspected three independent *PDX1.1* overexpression lines (Raschke et al., 2011). All three lines continued elongating their primary roots even after 6 days of ammonium exposure when root elongation of the wild type was almost completely exhausted (Figure 5A–5C). DAB staining showed that overexpression of *PDX1.1* strongly reduced the level of H_2O_2 in ammonium-treated primary roots (Figure 5D). Accordingly, ammonium-induced inhibition of root cortical cell length, meristem size, and activity of the *CycB1;1::GUS* reporter also recovered by overexpression of *PDX1.1* (Figure 5E–5G and Supplemental Figure 19), revealing the efficacy of endogenous vitamin B_6 formation under ammonium nutrition. Moreover, a $^{15}NH_4^+$ influx experiment revealed that the ammonium uptake capacity in roots remained unaffected in the *pdx1.1-3* mutant as well as in the *PDX1.1* overexpression lines (Figure 5H). Taken together, elevated expression of *PDX1.1* is sufficient to restore elongation in ammonium-exposed roots and acts downstream of the ammonium uptake process.

Overexpression of *PDX1.1* increases the level of non-phosphorylated B_6 vitamers

As the PDX1-dependent step in vitamin B_6 biosynthesis first yields PLP (Supplemental Figure 15), we hypothesized that overexpression of *PDX1.1* will primarily increase phosphorylated rather than non-phosphorylated vitamers, whose generation requires an additional phosphatase reaction. Measuring vitamin B_6 in roots confirmed significantly lower levels of total vitamin B_6 in the *pdx1.1-3* mutant than in the wild type, which was caused by a significant decrease in the concentrations of all five determined B_6 vitamers (Figure 6A and 6B). At first glance, this suggested a constitutive contribution of *PDX1.1* to overall vitamin B_6 biosynthesis because vitamin B_6 levels decreased in *pdx1.1-3* irrespective of the supplied N form. Overexpression of *PDX1.1* led to constitutively higher total vitamin B_6 levels only in *PDX1.1OE-L5*, but under ammonium supply also in *PDX1.1OE-L15* and to lesser extent in *PDX1.1OE-L8*, which coincided with elevated *PDX1.1* transcript levels in these lines (Figure 6A–6C). Surprisingly, the concentration of PLP was not enhanced in ammonium-supplied *PDX1.1* overexpression lines, although PLP contributed >70% to overall vitamin B_6 levels. In contrast, *PDX1.1* overexpression lines showed significantly higher concentrations of non-phosphorylated vitamin B_6 forms than the wild type, and these differences closely reflected the relative differences in transcript levels among the three overexpression lines. Hence, the proportion of individual B_6 vitamers shifted toward the non-phosphorylated vitamin B_6 forms, among which PL was the most abundant form, contributing up to 25% of total vitamin B_6 (Figure 6B). PM accounted only for approximately 1% of total vitamin B_6 in roots. In wild-type roots, 20% of total vitamin B_6 was in non-phosphorylated forms while in *pdx1.1-3* this proportion was less than 10%. In *PDX1.1* overexpression lines, between 30% and 40% of total vitamin B_6 was converted into non-phosphorylated forms, and this share even increased when plants were grown in the presence of ammonium (Figure 6A and 6B). We finally correlated the levels of individual B_6 vitamers with those of *PDX1.1* transcripts and revealed close correlations for PN, PL, and PM, but not for PMP, whereas the correlation for PLP was also significant although much weaker (Figure 6D). These results indicate that the extent of *PDX1.1* upregulation by ammonium or by ectopic expression determines primarily the abundance of non-phosphorylated B_6 vitamers without compromising homeostasis of phosphorylated B_6 vitamers in roots.

H_2O_2 triggers localized upregulation of *PDX1.1* under ammonium supply

To investigate the transcriptional regulation of vitamin B_6 biosynthesis and homeostasis by ammonium, we examined the transcript levels of all known genes involved in vitamin B_6 biosynthesis or metabolism by quantitative real-time PCR in roots grown under different N supply. Unexpectedly, *PDX1.1* turned out to be the sole vitamin B_6-related gene that was significantly upregulated by ammonium (Figure 7A). Next, the tissue-specific expression pattern of *PDX1.1* was monitored in plants expressing a *PDX1.1* promoter-GUS reporter construct (Boycheva et al., 2015). *PDX1.1* reporter activity was upregulated by ammonium supply in the root vasculature, increasing from the elongation zone basipetally through the differentiation zone (Figure 7B). As the reporter activity became stronger in the presence of 10 mM ammonium, upregulation of *PDX1.1* expression apparently followed ammonium supply in a dose-dependent manner (Figure 7A and 7B).

Since the spatial localization of *PDX1.1* expression and H_2O_2 accumulation strongly overlapped in ammonium-treated roots (Figures 2A, 2B, and 7B), the question arose as to whether

(E) Cell length and meristem size of primary roots of wild type, *pdx1.1-3*, and *PDX1.1OE-L5*. The length of mature cortical cells and the size of the root apical meristem are indicated by yellow arrowheads. DIC images of primary root tips were taken 6 days after treatment. Scale bars, 100 μm.
(F and G) Quantitative readout of mature cortical cell length **(F)** and primary root meristem size **(G)**. Boxes show the first quartile, median, and third quartile; whiskers show the minimum and maximum values, $n = 16$ plants. Different letters represent significant differences between lines and treatments according to two-way ANOVA followed by Tukey's HSD test, $P < 0.05$.
(H) Influx of $^{15}NH_4^+$ into roots of wild-type, *pdx1.1-3* mutant, and *PDX1.1* overexpression lines. Plants were pre-cultured hydroponically for 5 weeks and then subjected to N starvation for 4 days before being transferred to 200 μM ^{15}N-labeled NH_4^+ for 6 min. Bars represent means ± SD, $n = 5$ biological replicates. Asterisks denote significant differences between wild-type and indicated lines at $^*P < 0.05$ by Dunnett's multiple test; ns, not significant.

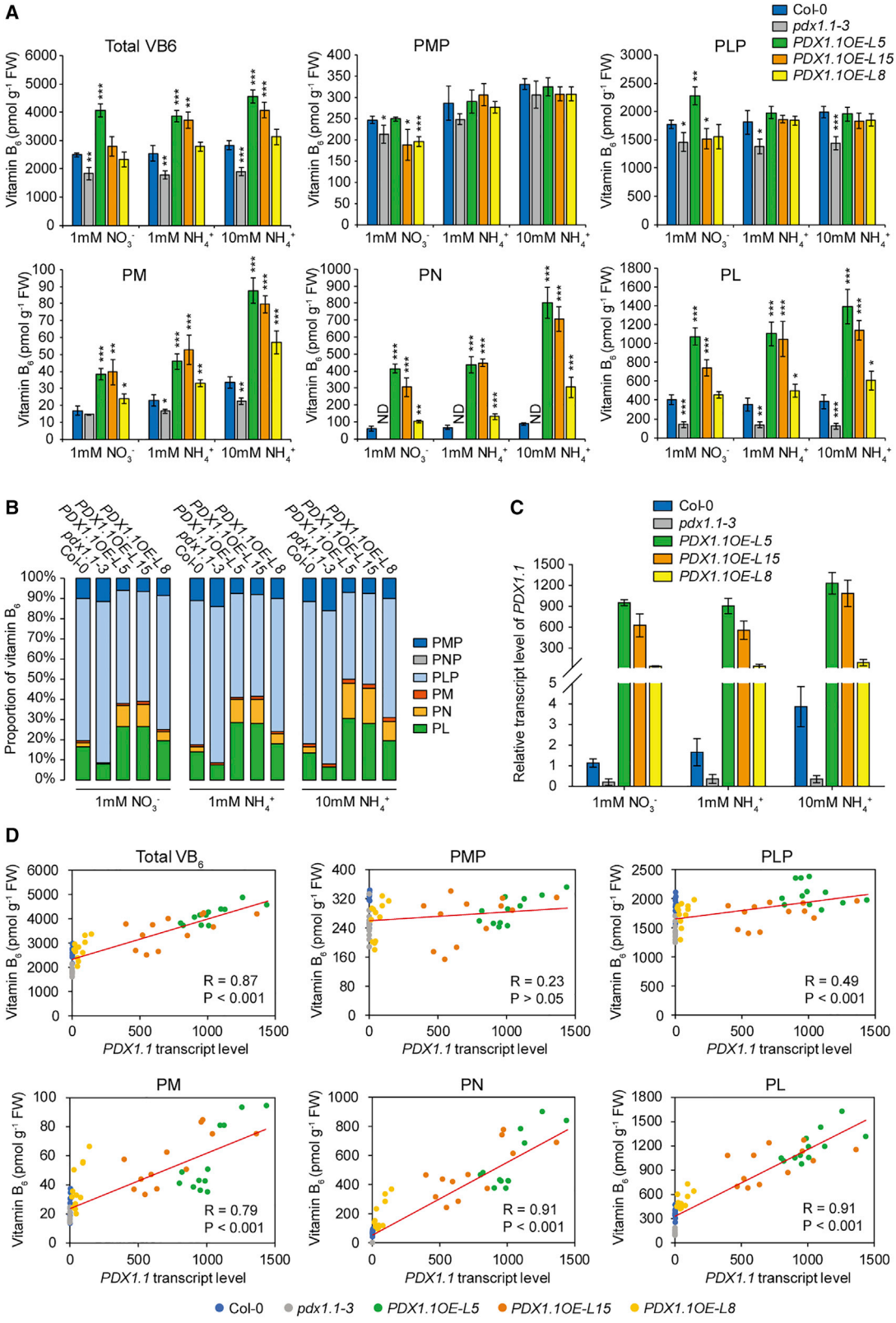

Figure 6. Vitamin B_6 profiling of *pdx1.1* mutant and *PDX1.1*-overexpressing plants under different N regimes.

(A) Root concentrations of vitamin B_6, pyridoxamine 5′-phosphate (PMP), pyridoxal 5′-phosphate (PLP), pyridoxamine (PM), pyridoxine (PN), and pyridoxal (PL) in wild-type (Col-0), *pdx1.1-3* mutant, and three *PDX1.1* overexpression lines 6 days after transfer to different N supply. The amount of

(legend continued on next page)

ammonium itself or H_2O_2 triggered the upregulation of *PDX1.1*. We thus suppressed H_2O_2 levels in ammonium-exposed roots by supply of KI or by low Fe and observed that *PDX1.1* reporter activity disappeared (Figure 7B). By contrast, exogenous application of 1 mM H_2O_2 strongly enhanced the promoter activity of *PDX1.1* in the root stele as well as in the apical root meristem, but only in the presence of ammonium (Figure 7C). Therefore, H_2O_2 serves as a signal to upregulate *PDX1.1* transcription upon ammonium nutrition and to determine its restricted expression in the stele.

Given that the change of pH upon ammonium exposure is the initial event to trigger the Fe-dependent oxidative burst, we hypothesized that the transcriptional response of *PDX1.1* to ammonium should be influenced by medium pH. Indeed, when *pPDX1.1*:*GUS* reporter lines were shifted from pH 5.7 to 5.0, the upregulation of *PDX1.1* was enhanced in the presence of ammonium. By contrast, when raising medium pH from 5.7 to 6.5 or 7.2, the induction of *PDX1.1* by ammonium almost disappeared (Supplemental Figure 20). These findings confirmed that ammonium- and pH-dependent H_2O_2 generation is required to induce the expression of *PDX1.1* in roots.

Elevation of PDX1.1-mediated vitamin B_6 biosynthesis improves plant tolerance to further nutrient-related stresses

Apart from ammonium toxicity, other nutrient-related stresses also arrest root elongation by elevated ROS formation, such as phosphate deficiency or nickel toxicity (Müller et al., 2015; Zheng et al., 2019; Lešková et al., 2020). We wondered whether PDX1.1-mediated vitamin B_6 biosynthesis also counteracts these oxidative stresses in plants. First, we inspected published transcriptome results (Bhosale et al., 2018; Lešková et al., 2020) to assess the response of vitamin B_6-related genes to phosphate deficiency and nickel toxicity. Surprisingly, none of the known genes involved in vitamin B_6 biosynthesis or metabolism, including *PDX1.1*, was differentially expressed under phosphate deficiency or nickel toxicity (Supplemental Figure 21A and 21B). Next, the arrest of primary root elongation under phosphate deficiency or nickel toxicity showed no difference between wild-type (Columbia-0 [Col-0]) and *pdx1.1-3* mutant plants (Supplemental Figure 21C–21F). These results suggested that vitamin B_6-dependent ROS protection did not evolve as a strategy to alleviate oxidative stress in response to phosphate deficiency or nickel toxicity in natural conditions. Nonetheless, coinciding with their enhanced ROS-scavenging capacity, all three *PDX1.1* overexpression lines exhibited significantly improved root elongation under phosphate deficiency or nickel toxicity (Supplemental Figure 21C–21F). This result suggests that enhanced *PDX1.1*-mediated vitamin B_6 biosynthesis can be applied as a practical strategy to improve root tolerance to multiple types of oxidative stress.

DISCUSSION

Application of ammonium-based N fertilizers in agricultural plant production bears the risk of impaired root development when roots are exposed to ammonium-rich soil patches (Britto and Kronzucker, 2002; Watt et al., 2006). Plants have evolved several strategies to cope with the adverse effects of predominant ammonium nutrition, which comprise enhanced N assimilation in roots (Cruz et al., 2006; Guan et al., 2016; Konishi et al., 2017), ammonium compartmentalization to the apoplast or vacuole (Loqué et al., 2005; Li et al., 2010; Bai et al., 2014), and activation of enzymatic anti-oxidation systems to cope with ammonium-triggered ROS production (Patterson et al., 2010; Xie et al., 2015). In this study, we describe the mechanistic basis underlying ammonium-triggered ROS formation and identify with PDX1.1-dependent vitamin B_6 synthesis a metabolic defense response to counteract ammonium-induced ROS formation.

Ammonium-dependent acidification triggers ROS formation via enhanced Fe mobilization

Ammonium toxicity belongs to one of several mineral element disorders that associate root growth inhibition with the production of ROS (Figure 1; Xie et al., 2015). Among these disorders, localization and generation of ROS differ in an element-specific manner, pointing to different sources of ROS formation. For instance, root growth inhibition by nickel has been related to ROS formation in outer cells of the apical root zone (Lešková et al., 2020), while ROS accumulate predominantly in the meristem and elongation zone under zinc deficiency (Nakayama et al., 2020) or in the root vasculature from the meristematic through the elongation and differentiation zone of salt-stressed plants (Jiang et al., 2012). Considering that experimental visualization and localization of ROS depend not only on the site of generation but also on chemical properties of the ROS-sensitive dye or reporter, we used here DAB staining and H_2DCFDA-dependent fluorescence to localize ROS formation under ammonium nutrition primarily to the vascular cylinder or stele in the elongation and differentiation zones (Figure 2). With increasing ammonium supply and time of exposure, ROS formation gradually progressed through the elongation zone toward the meristem (Figure 2B and 2C; Supplemental Figure 7B), where it coincided with suppressed cell length, meristem size, and cell division activity (Figure 1; Supplemental Figures 3 and 8), revealing that the apical root meristem is not the primary target of ammonium-dependent ROS generation especially at early stages of ammonium exposure. Although cytokinins are crucial in balancing cell division and meristem size (Dello Ioio et al., 2008), key components of cytokinin signaling are apparently not involved in ammonium-dependent root growth inhibition (Supplemental Figure 2).

pyridoxine 5′-phosphate (PNP) was too low to be detected in this study. Bars represent means ± SD, $n = 4$ independent biological replicates. Asterisks denote significant differences between wild-type and indicated lines at $^*P < 0.05$, $^{**}P < 0.01$, $^{***}P < 0.001$ by Dunnett's multiple test; ND, not detected.
(B and C) Proportion of individual B_6 vitamers in the roots **(B)** and relative transcript abundance of *PDX1.1* in the roots **(C)** of wild-type, *pdx1.1-3*, and *PDX1.1* overexpression lines 6 days after transfer to different N supplies. The relative transcript level of *PDX1.1* was determined by quantitative real-time PCR, and normalized by using *ACTIN2* and *UBQ10* as internal controls. Bars represent means ± SD, $n = 4$ independent biological replicates.
(D) Correlation between the transcript abundance of *PDX1.1* and the concentration of individual B_6 vitamers in roots of wild-type, *pdx1.1-3*, and *PDX1.1* overexpression lines. Pearson's correlation coefficients are shown as *R* values.

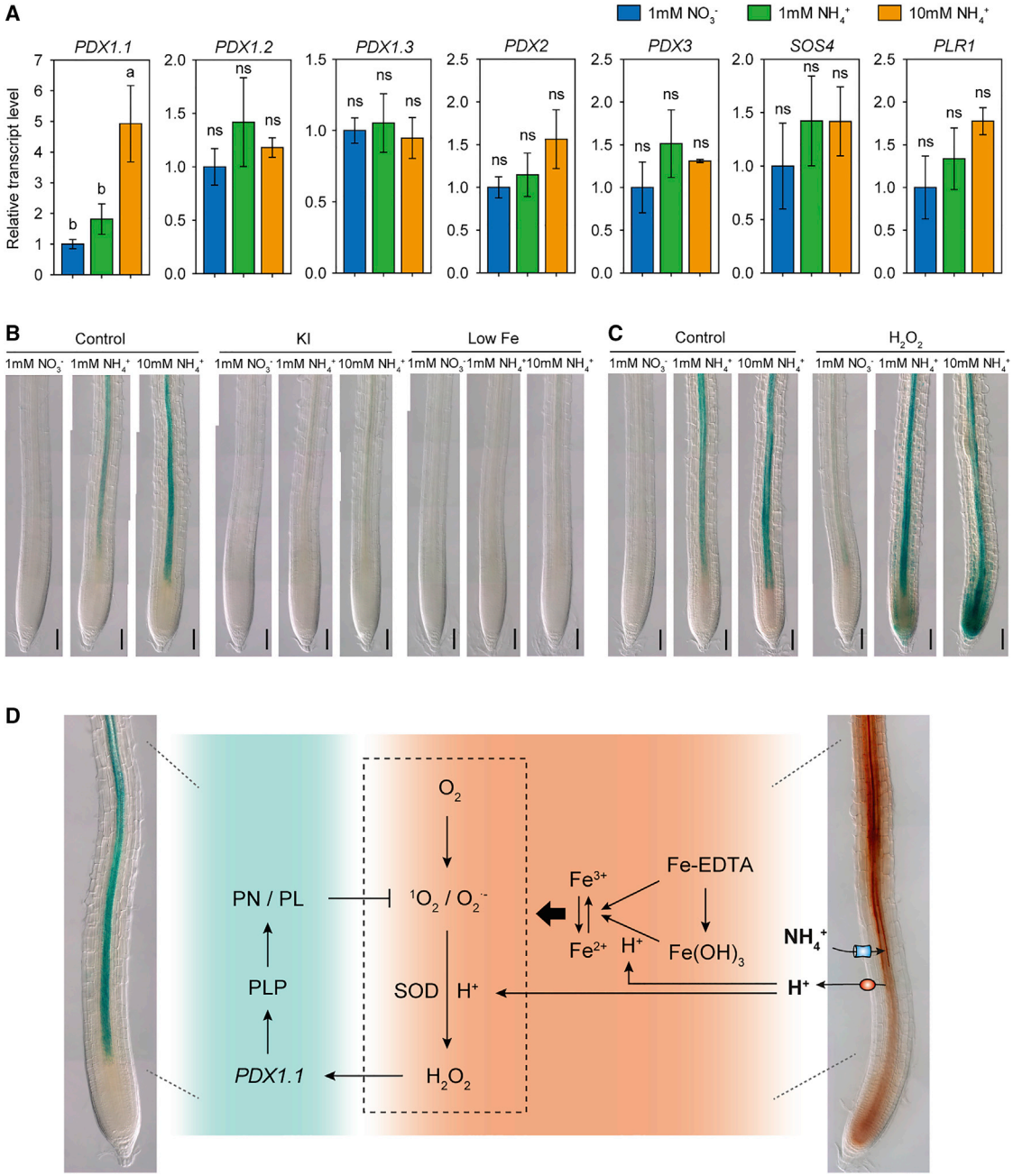

Figure 7. Transcriptional regulation of *PDX1.1* and other vitamin B_6-related genes in response to ammonium.

(A) Relative transcript abundance of *PDX1.1*, *PDX1.2*, *PDX1.3*, *PDX2*, *PDX3*, *SOS4*, and *PLR1* in roots of wild-type plants 6 days after transfer to different N supplies. Relative transcript levels were determined by quantitative real-time PCR and normalized by using both *ACTIN2* and *UBQ10* as multiple internal controls. Bars represent means ± SD, $n = 3$ biological replicates. Different letters represent significant differences among means at $P < 0.05$ according to Tukey's HSD test; ns, not significant.

(B and C) Promoter activity of the *pPDX1.1*:*GUS* reporter in primary roots 6 days after transfer to different N treatments in the absence or presence of 0.5 mM KI or under supply of 10 μM Fe(III)-EDTA (low Fe) **(B)** or in the presence of 1 mM H_2O_2 **(C)**. Representative images from 10 plants per treatment are shown. Scale bars, 100 μm.

(D) A working model deciphering the role of ammonium-triggered proton release in Fe-dependent ROS metabolism and subsequent vitamin B_6 formation. Ammonium uptake provokes proton secretion and apoplastic acidification, which increases Fe solubilization in the root apoplast and the rhizosphere along the elongation and differentiation zones of the root. Secreted protons (i) mobilize Fe from ETDA or the apoplastic Fe pool ($Fe(OH)_3$) and (ii) enable superoxide dismutase (SOD)-mediated conversion of superoxide ($O_2^{\cdot -}$) to H_2O_2. H_2O_2 upregulates *PDX1.1* expression to enhance accumulation of non-phosphorylated B_6 vitamers, in particular pyridoxine (PN) and pyridoxal (PL), which serve as antioxidants quenching the reactive molecular oxygen species $^1O_2$ or ($O_2^{\cdot -}$). The root images on the right and left side refer to the primary root tips of DAB-stained seedlings and *pPDX1.1*:*GUS* reporter lines under ammonium supply, respectively.

Since ammonium-dependent root growth inhibition was suppressed when H_2O_2 accumulation was chemically quenched by KI (Figure 1) but enhanced when H_2O_2 accumulation was favored in the presence of SHAM or by H_2O_2 supplementation (Supplemental Figure 3), H_2O_2 or a downstream product must have caused the stunted root phenotype. This is supported by the observation that blocking H_2O_2 formation by DDC in favor of $O_2^{\cdot-}$ accumulation prevented ammonium-dependent root growth inhibition (Supplemental Figure 4). On the other hand, high effectiveness of SOD inhibition by DDC implied that DAB-stained H_2O_2 was generated via $O_2^{\cdot-}$, which in turn may derive from peroxisomes and the mitochondrial electron transport chain or from the activity of NADPH oxidases in the plasma membrane (Smirnoff and Arnaud, 2018). By examining a limited number of available *rboh* single or multiple knockout lines, we could not find evidence for a role of RBOH-type NADPH oxidases in ammonium-triggered root growth inhibition (Supplemental Figure 5), even though our assay also included the root stele-localized RBOH F, which triggers vascular ROS formation upon salinity as a prerequisite for salt tolerance (Jiang et al., 2012). Irrespective of the $O_2^{\cdot-}$ source, SOD-mediated dismutation of $O_2^{\cdot-}$ to H_2O_2 consumes protons and is favored by low apoplastic pH (Smirnoff and Arnaud, 2018) that resulted here from ammonium uptake-induced proton secretion (Figures 2 and 7D; Meier et al., 2020). Suppressed DAB staining and mitigation of root growth inhibition under low Fe supply (Figure 1) indicated a key role of Fe in H_2O_2 formation. Indeed, exposure of ammonium-grown roots to light, which increases the pool of redox-active Fe (Zheng et al., 2019), aggravated inhibition of root elongation (Supplemental Figure 12). Furthermore, redox-active Fe(III) likely arose from apoplastic acidification and dissolution of apoplastic Fe pools (Supplemental Figure 6; Zhu et al., 2018) as well as from UV-dependent photo-oxidation of EDTA that sets chelated ferric Fe free (Hangarter and Stasinopoulos, 1991). A similarly critical role of ferrous Fe in ROS-mediated root growth inhibition is also known for primary root growth inhibition under phosphate starvation (Müller et al., 2015; Zheng et al., 2019). In this context, exposure of P-deficient roots to light favors reduction of ferric to ferrous Fe and subsequent Fe^{2+}-mediated formation of hydroxyl radicals via the Fenton reaction. DAB-stained H_2O_2 under phosphorus (P) deficiency is confined to the meristematic root zone and further depends on malate efflux via ALMT1 (Zheng et al., 2019) to increase Fe solubility in the apoplast (Balzergue et al., 2017; Mora-Macías et al., 2017). Since the root elongation in response to ammonium was not altered in *almt1* mutants (Supplemental Figure 14A and 14B), root shading restored root elongation only in part (Supplemental Figure 12), and ammonium-dependent H_2O_2 mainly localized to the root stele above the meristematic zone (Figure 2), mechanisms underlying ROS formation clearly differ between P-deficient and ammonium-exposed roots. Moreover, supplementation of the hydroxyl radical scavenger thiourea, which can restore arrested primary root elongation under P deficiency (Zheng et al., 2019), was poorly effective in the case of ammonium (Supplemental Figure 13), suggesting that formation of hydroxyl radicals via the Fenton reaction is not critical for ammonium-dependent root growth inhibition. Nonetheless, a determinant role of redox-active Fe in ammonium-triggered root growth inhibition is corroborated by its gradual relief under increasing medium pH, which also decreased Fe accumulation in the root and subsequent Fe availability for ROS metabolism (Figure 3). We thus conclude that ammonium-induced acidification of the root apoplast and additionally in the rhizosphere enhance Fe solubilization as prerequisite for relocation to the stele and subsequent Fe-mediated formation of H_2O_2.

Plant roots counteract ammonium-induced ROS formation via PDX1.1-mediated vitamin B_6 biosynthesis

In plants, vitamin B_6 is synthesized via the "deoxyxylulose-5-phosphate (DXP)-independent pathway," which utilizes ribose-5-phosphate, glyceraldehyde-3-phosphate, and glutamine as substrates for the glutamine amidotransferase complex comprising pyridoxine synthase (PDX1) and pyridoxine glutaminase (PDX2) (Tambasco-Studart et al., 2005). The primary product is the phosphorylated form PLP (Tambasco-Studart et al., 2005) before enzymes of the salvage pathway facilitate the interconversion among different B_6 vitamers (Colinas et al., 2016; Supplemental Figure 15). While PLP acts as coenzyme in numerous enzymatic reactions, including those with importance for N assimilation (Percudani and Peracchi, 2003; Fitzpatrick, 2011; Colinas et al., 2016), non-phosphorylated forms of vitamin B_6 serve efficiently as antioxidants *in vitro* and *in vivo* (Bilski et al., 2000; Havaux et al., 2009; Mooney and Hellmann, 2010). Our study provides several lines of evidence indicating that plants induce PDX1.1-mediated synthesis of non-phosphorylated B_6 vitamers as an efficient strategy to counteract ammonium-dependent oxidative stress in roots.

First, as several enzymes are required for vitamin B_6 biosynthesis and homeostasis, it was surprising that only one of them, *PDX1.1*, responded to ammonium with enhanced expression (Figure 7A). Indeed, overexpression of *PDX1.1* suppressed ammonium-dependent H_2O_2 formation and associated root length inhibition, whereas *pdx1.1* mutant lines were hypersensitive to ammonium (Figures 4 and 5; Supplemental Figure 14). As in these lines total vitamin B_6 levels closely followed *PDX1.1* transcript levels in roots, transcriptional regulation of PDX1.1-dependent PLP synthesis alone provides sufficient plasticity to counteract the adverse growth effect of ammonium. Among the three paralogs of PDX1 in *Arabidopsis*, only PDX1.1 and PDX1.3 show catalytic activities (Tambasco-Studart et al., 2005), while *PDX1.2* encodes a pseudoenzyme that can boost vitamin B_6 biosynthesis via heteromerization with its paralogs in response to singlet oxygen or heat stress (Moccand et al., 2014). Although spatial and temporal expression patterns of *PDX1.1* and *PDX1.3* largely overlap and only disruption of both genes causes embryo lethality, PDX1.3 has been found to be more abundant and requisite for stress tolerance than PDX1.1 (Titiz et al., 2006). Nonetheless, enhanced expression of PDX1.3 at the protein level appears to require PDX1.2 (Dell'Aglio et al., 2017), whereas overexpression of PDX1.1 can be achieved with the protein alone to substantially increase vitamin B_6 production (Raschke et al., 2011; Figure 6). This regulatory versatility of PDX1.1 may provide an advantage when plants need to respond instantly to oxidative stresses.

Second, external supply of vitamin B_6 to *pdx1.1-3* mutant or wild-type plants completely prevented ammonium-induced inhibition of root elongation (Figure 4). Although the overall vitamin B_6

level in the *pdx1.1-3* mutant line was only 20%–30% lower than in the wild type (Figure 6A), this difference as well as a further 50%–100% increase in the overexpressing lines gradually improved root growth, indicating a strong dose dependence of beneficial vitamin B_6 action. This dose-dependent effect went back to the abundance of the non-phosphorylated B_6 vitamers (Figure 6A), because only PL and PN restored root length while the primary biosynthesis product PLP remained ineffective (Supplemental Figure 18). Superior functionality of non-phosphorylated vitamers as ROS scavengers is most likely determined by substituents of the pyridoxine core that modulate electron density in the ring and thus the interaction with singlet molecular oxygen ($^1O_2$; Bilski et al., 2000). Upon quenching of $^1O_2$ the pyridoxine ring is degraded (Bilski et al., 2000), explaining the dose-dependent rather than catalytic effect of vitamin B_6 as observed here (Figures 5 and 6). Since in overexpression lines root concentrations of only the three non-phosphorylated vitamers PM, PN, and PL correlated closely with *PDX1.1* transcript levels (Figure 6D), transcriptional upregulation of *PDX1.1* is sufficient to confer a B_6 vitamer-specific defense response to stress.

Third, *PDX1.1*-mediated biosynthesis *de novo* of vitamin B_6 spatially and temporally coincides with ammonium-induced ROS formation in roots. Within a time frame of a few days, there was a robust temporal coincidence between root elongation rates and H_2O_2 accumulation, even when vitamin B_6 was provided externally or *PDX1.1* expression levels were modulated (Figures 4 and 5). Also at the tissue level, spatial patterns of *PDX1.1* transcript levels and H_2O_2 accumulation strongly overlapped in ammonium-treated roots (Figures 2 and 7), supporting the notion that vitamin B_6 biosynthesis is targeted to those tissues and root developmental zones that are most severely affected by ROS accumulation. In plants, biosynthesis *de novo* of vitamin B_6 relies on PDX2 using glutamine as a substrate to produce PLP (Supplemental Figure 15; Tambasco-Studart et al., 2005; Fitzpatrick et al., 2007; Boycheva et al., 2015). Glutamine is also the most abundant product of ammonium assimilation in roots (Xu et al., 2012; Liu and von Wirén, 2017), which is mediated by cytosolic glutamine synthetase. Interestingly, GLN1;2-mediated glutamine synthesis preferentially localizes in the root vasculature, and GLN1;2 represents the most strongly upregulated GLN isoform in ammonium-supplied roots (Ishiyama et al., 2004; Lothier et al., 2011; Guan et al., 2016). Alternatively, ammonium may also be used directly by PDX1.1, independently of PDX2 action, as has been demonstrated *in vitro* (Raschle et al., 2007). In this context, elevated availability not only of glutamine but also of ammonium as one educt for vitamin B_6 synthesis in those cells that suffer most from ROS production may be a factor in why plants favored vitamin B_6 as preferential ROS scavenger during evolutionary adaptation to elevated external ammonium levels. Given that ammonium-induced ROS formation occurs in all cell types of the root differentiation zone and meristem (Figure 2A–2C and Supplemental Figure 7B) while the enhancement of PDX1.1-mediated vitamin B_6 biosynthesis under ammonium supply is confined to the vasculature (Figure 7B and Supplemental Figure 20), the question arises as to how root cells that do not produce vitamin B_6 are protected from oxidative stress. Likely there is a radial transport pathway bringing vitamin B_6 from the vasculature to the outer root cells, driven either by diffusion of non-phosphorylated B_6 vitamers that are considered able to permeate membranes (Stolz and Vielreicher, 2003), or by radial transport via membrane proteins such as purine permeases (PUPs). In particular, PUP1 has been shown to transport non-phosphorylated B_6 vitamers in *Arabidopsis* as well as after heterologous expression in yeast (Szydlowski et al., 2013).

Vitamin B_6 has proven effectiveness in ROS detoxification in a variety of systems and conditions. In different human cell cultures, the supplementation of non-phosphorylated forms of vitamin B_6 alleviates superoxide-induced damage and lipid peroxidation (Jain and Lim, 2001; Kannan and Jain, 2004; Mahfouz et al., 2009). In *Arabidopsis* protoplasts, PN supplementation can reduce oxidative damage generated upon high illumination (Danon et al., 2005). When leaf disks were exposed directly to $^1O_2$, lipid peroxidation in the *pdx1.3* background was higher than in the wild type (Havaux et al., 2009). Since this effect was not observed with $O_2^{\cdot-}$ or H_2O_2, and since $^1O_2$ levels rise during illumination more drastically in the *pdx1.3* mutant than in the wild type, vitamin B_6 has been proposed to act as $^1O_2$ quencher (Danon et al., 2005; Havaux et al., 2009). Moreover, $^1O_2$ can easily convert to $O_2^{\cdot-}$ by electron transfer (Khan and Kasha, 1994) and is further converted to H_2O_2 by SOD, allowing reactive Fe to take in a key role in ammonium-induced ROS processing (Figure 7D). Our study could not identify the source of produced $^1O_2$ or $O_2^{\cdot-}$ species, as analysis of a few tested *rboh* mutants did not provide sufficient evidence to rule out NADPH oxidases as a source for $O_2^{\cdot-}$ formation (Supplemental Figure 5). Alternatively, $^1O_2$ or $O_2^{\cdot-}$ species may derive from electron transport processes in root plastids or mitochondria (Smirnoff and Arnaud, 2018). Irrespective of their origin, their accumulation during repression of SOD by DDC was ineffective in inhibiting root elongation (Supplemental Figure 4), indicating that the conversion of $O_2^{\cdot-}$ to H_2O_2 by SOD was required to inhibit root elongation (Figure 7D). In fact these two ROS species greatly influence root development by regulating the balance between cell proliferation and cell differentiation in the root tips (Tsukagoshi, 2016). Specifically, $O_2^{\cdot-}$ localized in the meristematic zone maintains cell division while H_2O_2 prevailing in the elongation zone stimulates cell differentiation (Tsukagoshi et al., 2010). However, excessive accumulation of H_2O_2 in the elongation zone leads to a repression of root growth reflected by inhibited cell elongation and smaller meristem size (Tsukagoshi et al., 2010). This may explain how H_2O_2 accumulation inhibited root elongation in ammonium-grown plants (Figure 7D).

Based on our study, we propose a working model of the processes underlying primary root growth inhibition under ammonium nutrition (Figure 7D). Ammonium uptake, which is particularly high in the elongation zone (Duan et al., 2018), provokes apoplastic acidification (Meier et al., 2020) that increases Fe solubilization and reprecipitation in inner root cells (Figures 2 and 7D). It is not yet completely clear why Fe preferentially accumulates along the stele and whether the required change in Fe binding forms for xylem loading is involved, but previous studies have confirmed enhanced Fe precipitation in the pericycle and xylem (Green and Rogers, 2004; Roschzttardtz et al., 2009). There, elevated Fe availability and acidic pH favor $O_2^{\cdot-}$ dismutation and H_2O_2 formation (Smirnoff and Arnaud, 2018; Figure 7D). Considering that ammonium uptake-dependent acidification stimulates the

generation of H_2O_2, H_2O_2 or a downstream product induces *PDX1.1* expression at the site of Fe and ROS localization (Figure 7B and 7D). Predominant biosynthesis of non-phosphorylated B_6 vitamers (Figure 6) can subsequently quench reactive molecular oxygen ($^1O_2/O_2^{\cdot-}$) that serves as a source for H_2O_2 formation (Supplemental Figure 4) and thereby counteract ammonium-induced H_2O_2 formation to restore root growth. We find that this PDX1.1-mediated biosynthesis *de novo* of vitamin B_6 is not only essential for protecting roots against ammonium toxicity, as occurring in ammonium-enriched fertilizer bands in agricultural plant production, but is also effective against other adverse growth conditions that involve Fe-dependent ROS formation such as P deficiency and nickel toxicity.

METHODS

Plant materials and growth conditions

Arabidopsis thaliana accession Col-0 and Ler served as wild type. The following mutants and transgenic lines were used: *ahk3-3* (Dello Ioio et al., 2007), *arr1-3* (Dello Ioio et al., 2007), *arr12-1* (Dello Ioio et al., 2007), *shy2-31* (Dello Ioio et al., 2008), *shy2-2* (Dello Ioio et al., 2008), *TCS:GFP* (Bielach et al., 2012), *pdx1.1-1* (Titiz et al., 2006), *pdx1.1-3* (SALK_024245), *apo-pHusion* (Gjetting et al., 2012), *PDX1.1OE-L5* (Raschke et al., 2011), *PDX1.1OE-L8* (Raschke et al., 2011), *PDX1.1OE-L15* (Raschke et al., 2011), *pPDX1.1:GUS* (Boycheva et al., 2015), and *CycB1;1::GUS* (Colón-Carmona et al., 1999). The cell-cycle reporter *CycB1;1::GUS* (Col-0 background) was introduced into *pdx1.1-3* or *PDX1.1OE-L5* by crossing to generate *CycB1;1::GUS* (*pdx1.1-3*) and *CycB1;1::GUS* (*PDX1.1OE-L5*) lines. Complete information regarding T-DNA insertion lines of 29 ammonium-responsive genes used in the mutagenesis screen are listed in Supplemental Data 1. *Arabidopsis* seeds were surface sterilized by 70% ethanol with 0.05% (v/v) Triton X-100, cultured on modified half-strength MS medium containing 100 μM Fe(III)-EDTA, 0.5% sucrose, 1% Duchefa Phyto agar (Duchefa Biochemie), and 2.5 mM MES (pH 5.7), and N sources were added to different final concentrations as described in the figure legends. Seedlings grown in Petri dishes (12 × 12 cm) were cultured vertically in a growth chamber under a 22°C/18°C and 10-h/14-h (light/dark) regime at light intensity of 120 μmol photons m^{-2} s^{-1}. For root phenotyping experiments, plants were pre-cultured on half-strength MS medium containing 1 mM KNO_3 for 6 days and then transferred to treatment plates supplemented with half-strength MS medium containing 1 mM KNO_3, 1 mM NH_4Cl, or 10 mM NH_4Cl, respectively. K_2SO_4 (0.5 mM) was added to balance K^+ concentration in the ammonium treatment. Root phenotypes were measured 6 days after transfer. To generate P deficiency, we transferred 6-day-old plants to half-strength MS medium containing 625 μM KH_2PO_4 (+P) or 5 μM KH_2PO_4 (−P), and added KCl to −P medium to balance K^+ concentrations. For Ni toxicity, 6-day-old plants were transferred to half-strength MS medium in the absence (−Ni) or presence (+Ni) of 75 μM $NiSO_4$. Root phenotypes were assessed 6 days after transfer. When supplementing H_2O_2, fresh 30% H_2O_2 (Roth) solution (9.79 mol l^{-1}) was diluted to a concentration of 1 M and supplied to the medium after autoclaving. In the root shading experiment, root-containing segments of Petri dishes were covered with aluminum foil as described in Zheng et al. (2019). For vitamin B_6 supplementation experiments, different B_6 vitamers were dissolved in water and supplied to agar medium at a final concentration of 5 μM. Key chemical information is given in Supplemental Table 1.

Root growth measurements

During root phenotyping experiments, the position of primary roots was labeled every day after treatment in order to calculate primary root elongation rate. Root images were taken by an Epson 10000XL scanner at a resolution of 300 dpi. Primary root growth parameters were measured by WinRHIZO Pro 2007 software (Regents Instruments, Canada). Differential interference contrast (DIC) microscopy images of primary root tips were taken to assess the size of primary root meristem and the length of mature cortical cell as described in Dello Ioio et al. (2007). All of the experiments were performed at least twice with similar results.

ROS detection

H_2O_2 in primary root tips were detected by DAB staining as described by Thordal-Christensen et al. (1997). In brief, primary roots were incubated in 1 mg ml^{-1} DAB solution for 8 h and then imaged by DIC microscopy. H_2O_2 is visualized as a reddish-brown coloration. A cell-permeant fluorogenic dye, H_2DCFDA, was also used to measure ROS activity in primary roots. Seedlings were stained for 20 min in a solution of 50 μM H_2DCFDA in 50 mM potassium phosphate buffers (pH 7.0). DCF fluorescence was excited at 488 nm and detected at 517–527 nm. Virtual color images were generated by a rainbow color code to indicate the fluorescence intensity of DCF in roots.

Apoplastic and rhizosphere pH measurements

Apoplastic pH changes were measured by the ratiometric pH reporter apo-pHusion (Gjetting et al., 2012). The fluorescence intensity ratio between pH-sensitive GFP and pH-insensitive RFP was calculated to indicate the changes of apoplastic pH, and virtual ratio images were generated by ImageJ v1.53 software. The changes of rhizosphere pH under different N supply were monitored by the pH indicator bromocresol purple (BCP), which changes color from yellow at pH 5.0 to violet at pH 7.2 (Meier et al., 2020). Six days after growth on different N sources, agar medium containing six seedlings per plate were stained overnight (18 h) with BCP solution at a final concentration of 0.1 mg ml^{-1}.

Histological staining

Promoter-driven GUS activity was determined by GUS staining as described previously (Li, 2011). Roots were rinsed once with staining buffer containing 50 mM $NaHPO_4$ buffer (pH 7.2), 2 mM potassium ferrocyanide, and 2 mM potassium ferricyanide, and incubated at 37°C in staining solution containing 2 mM X-Gluc. After staining, roots were cleared by HCG solution (chloral hydrate/water/glycerol = 8:3:1) and imaged by DIC microscopy. To assess the size of the primary root meristem and the length of mature cortical cell, we cleared non-staining primary root tips by HCG solution and imaged them by DIC microscopy. For staining of Fe accumulation in roots, a Perls staining and DAB/H_2O_2 intensification was performed according to Roschzttardtz et al. (2009). Roots were rinsed three times with 10 mM EDTA and then incubated for 5 min in a freshly prepared Perls staining solution. Thereafter, roots were incubated in a methanol solution containing 0.01 M NaN_3 and 0.3% (v/v) H_2O_2 for 1 h at room temperature. After washing three times with 0.1 M phosphate buffer (pH 7.4), roots were finally incubated for 5 min in an intensification solution containing 0.025% (w/v) DAB and 0.005% (v/v) H_2O_2 in 0.1 M phosphate buffer (pH 7.4). Roots were mounted with HCG solution before imaging by light microscopy.

Microscopy analyses

Fluorescent images were taken by a laser scanning confocal microscope (Zeiss LSM 780). Root samples were stained with 10 μg ml^{-1} propidium iodide (PI) for 5 min to visualize cell walls. GFP was excited at 488 nm and detected at 505–535 nm; RFP was excited at 561 nm and detected at 580–630 nm; PI was excited at 561 nm and detected at 600–700 nm; DCF fluorescence was excited at 488 nm and detected at 517–527 nm. The same microscope settings were kept to measure all confocal sections across samples. Fluorescence quantification of apo-pHusion and H_2DCFDA were conducted by Zeiss ZEN microscope software (version 2.6). Virtual ratio images were generated by ImageJ 1.53 software. DAB staining, Perls staining, GUS staining, and DIC imaging were conducted by a Zeiss Axio Imager 2 system. For light microscopy of *in situ*-localized Fe, root cuttings of 5 mm length of five seedlings from each growth condition were dissected approximately 1 cm above the root tip and subjected to aldehyde fixation, dehydration, and resin embedding as

described in Supplemental Table 2. Semi-thin sections of 2.5 μm thickness were cut with a Leica UCT microtome (Leica Microsystems, Wetzlar, Germany), and mounted on slides in rapid mounting medium Entelan (Sigma-Aldrich, Darmstadt, Germany). Sections were recorded with a 40× lens at fixed exposure time using a Zeiss Axio Imager M2 (Carl Zeiss Microscopy, Oberkochen, Germany).

Vitamin B_6 quantification analysis

The abundance of all individual B_6 vitamers in roots was determined by high-performance liquid chromatography. Vitamin B_6 quantification analyses were performed as described previously (Colinas et al., 2016) with the following changes: two separate extractions were performed with 15 volumes and 8 volumes of 50 mM ammonium acetate (pH 4.0), respectively, and a 50 μl injection volume was used for a single run per extract.

Real-time quantitative PCR

Total RNA was extracted from 10–20 mg of frozen root samples by an RNeasy plant mini kit (Qiagen) following the manufacturer's protocol. Template cDNA was synthesized from 1 μg of total RNA using SuperScript II Reverse Transcriptase (Thermo Fisher Scientific) and Oligo d(T)12-18 primer. Quantitative real-time PCR was performed by a CFX384 Touch Real-Time PCR Detection System (Bio-Rad) using iQ SYBR Green Supermix (Bio-Rad). According to the multiple internal control method (Vandesompele et al., 2002), relative transcript levels of target genes were calculated by the geNorm algorithm (https://genorm.cmgg.be), using *UBQ10* (*AT4G05320*) and *ACTIN2* (*AT3G18780*) as the multiple internal control genes in this study. Gene-specific primers for quantitative PCR are listed in Supplemental Table 3.

Statistical analysis

Data were collected and analyzed by Microsoft Excel 2016. Statistical analyses were conducted by GraphPad Prism 8 (version 8.3.0). Two-tailed Student's *t*-test, Dunnett's multiple test, or Tukey's HSD test was performed to test the statistical significance, and the *P* values of each statistical analysis are noted in the figure legends. Graphs were plotted by GraphPad Prism 8 (version 8.3.0) and edited by Adobe Illustrator 2020 (version 24.2.1).

ACCESSION NUMBERS

Sequence data in this study can be found in The Arabidopsis Information Resource according to the following accession numbers: *PDX1.1* (*AT2G38230*), *PDX1.2* (*AT3G16050*), *PDX1.3* (*AT5G01410*), *PDX2* (*AT5G60540*), *PDX3* (*AT5G49970*), *SOS4* (*AT5G37850*), *PLR1* (*AT5G53580*), *UBQ10* (*AT4G05320*), and *ACTIN2* (*AT3G18780*).

SUPPLEMENTAL INFORMATION

Supplemental information is available at *Molecular Plant Online*.

FUNDING

This work was supported by the Deutsche Forschungsgemeinschaft (Germany) with a grant (WI1728/13-2) to N.v.W. The Swiss National Science Foundation is also acknowledged for funding to T.B.F. (grants 31003A_14117 and IZLIZ3_183193).

AUTHOR CONTRIBUTIONS

Y.L. and N.v.W. conceived the project and designed the experiments. Y.L., R.F.H.G., R.A.M., M.M., P.S., and T.B.F. performed the experiments and analyzed the data. G.K. provided the transcriptome data. Y.L. and N.v.W. wrote the manuscript with the support of R.F.H.G. and T.B.F.

ACKNOWLEDGMENTS

We thank Twan Rutten (IPK Gatersleben) for microscopy advice. We thank Markus Meier, Cevza Esin Tunc, and Mohammad-Reza Hajirezaei (IPK Gatersleben) for scientific advice and valuable discussions. We further thank Jacqueline Fuge, Annett Bieber, Elis Fraust, Barbara Kettig, Yudelsy Antonia Tandron Moya, Dagmar Böhmert, and Christine Bethmann (IPK Gatersleben) for excellent technical assistance. No conflict of interest declared.

Received: June 2, 2021
Revised: November 5, 2021
Accepted: January 17, 2022
Published: January 18, 2022

REFERENCES

Auh, C.K., and Murphy, T.M. (1995). Plasma-membrane redox enzyme is involved in the synthesis of O_2^- and H_2O_2 by phytophthora elicitor-stimulated rose cells. Plant Physiol. **107**:1241–1247.

Bai, L., Ma, X., Zhang, G., Song, S., Zhou, Y., Gao, L., Miao, Y., and Song, C.P. (2014). A receptor-like kinase mediates ammonium homeostasis and is important for the polar growth of root hairs in *Arabidopsis*. Plant Cell **26**:1497–1511.

Balzergue, C., Dartevelle, T., Godon, C., Laugier, E., Meisrimler, C., Teulon, J.M., Creff, A., Bissler, M., Brouchoud, C., Hagege, A., et al. (2017). Low phosphate activates STOP1-ALMT1 to rapidly inhibit root cell elongation. Nat. Commun. **8**:15300.

Bhosale, R., Giri, J., Pandey, B.K., Giehl, R.F.H., Hartmann, A., Traini, R., Truskina, J., Leftley, N., Hanlon, M., Swarup, K., et al. (2018). A mechanistic framework for auxin dependent *Arabidopsis* root hair elongation to low external phosphate. Nat. Commun. **9**:1409.

Bielach, A., Podlesakova, K., Marhavy, P., Duclercq, J., Cuesta, C., Muller, B., Grunewald, W., Tarkowski, P., and Benkova, E. (2012). Spatiotemporal regulation of lateral root organogenesis in *Arabidopsis* by cytokinin. Plant Cell **24**:3967–3981.

Bilski, P., Li, M.Y., Ehrenshaft, M., Daub, M.E., and Chignell, C.F. (2000). Vitamin B6 (pyridoxine) and its derivatives are efficient singlet oxygen quenchers and potential fungal antioxidants. Photochem. Photobiol. **71**:129–134.

Boycheva, S., Dominguez, A., Rolcik, J., Boller, T., and Fitzpatrick, T.B. (2015). Consequences of a deficit in vitamin B6 biosynthesis de novo for hormone homeostasis and root development in *Arabidopsis*. Plant Physiol. **167**:102–117.

Britto, D.T., and Kronzucker, H.J. (2002). NH_4^+ toxicity in higher plants: a critical review. J. Plant Physiol. **159**:567–584.

Chu, X., Wang, J.G., Li, M., Zhang, S., Gao, Y., Fan, M., Han, C., Xiang, F., Li, G., Wang, Y., et al. (2021). HBI transcription factor-mediated ROS homeostasis regulates nitrate signal transduction. Plant Cell **33**:3004–3021.

Colinas, M., Eisenhut, M., Tohge, T., Pesquera, M., Fernie, A.R., Weber, A.P.M., and Fitzpatrick, T.B. (2016). Balancing of B-6 vitamers is essential for plant development and metabolism in *Arabidopsis*. Plant Cell **28**:439–453.

Colón-Carmona, A., You, R., Haimovitch-Gal, T., and Doerner, P. (1999). Spatio-temporal analysis of mitotic activity with a labile cyclin-GUS fusion protein. Plant J. **20**:503–508.

Cruz, C., Bio, A.F.M., Dominguez-Valdivia, M.D., Aparicio-Tejo, P.M., Lamsfus, C., and Martins-Loucao, M.A. (2006). How does glutamine synthetase activity determine plant tolerance to ammonium? Planta **223**:1068–1080.

Danon, A., Miersch, O., Felix, G., Camp, R.G., and Apel, K. (2005). Concurrent activation of cell death-regulating signaling pathways by singlet oxygen in *Arabidopsis thaliana*. Plant J. **41**:68–80.

Dell'Aglio, E., Boycheva, S., and Fitzpatrick, T.B. (2017). The pseudoenzyme PDX1.2 sustains vitamin B-6 biosynthesis as a function of heat stress. Plant Physiol. **174**:2098–2112.

Dello Ioio, R., Linhares, F.S., Scacchi, E., Casamitjana-Martinez, E., Heidstra, R., Costantino, P., and Sabatini, S. (2007). Cytokinins

determine *Arabidopsis* root-meristem size by controlling cell differentiation. Curr. Biol. **17**:678–682.

Dello Ioio, R., Nakamura, K., Moubayidin, L., Perilli, S., Taniguchi, M., Morita, M.T., Aoyama, T., Costantino, P., and Sabatini, S. (2008). A genetic framework for the control of cell division and differentiation in the root meristem. Science **322**:1380–1384.

Dixon, S.J., and Stockwell, B.R. (2014). The role of iron and reactive oxygen species in cell death. Nat. Chem. Biol. **10**:9–17.

Dong, Q., Bai, B., Almutairi, B.O., and Kudla, J. (2021). Emerging roles of the CBL-CIPK calcium signaling network as key regulatory hub in plant nutrition. J. Plant Physiol. **257**:153335.

Duan, F., Giehl, R.F.H., Geldner, N., Salt, D.E., and von Wirén, N. (2018). Root zone-specific localization of AMTs determines ammonium transport pathways and nitrogen allocation to shoots. PLOS Biol. **16**:e2006024.

Ferreira, F.J., and Kieber, J.J. (2005). Cytokinin signaling. Curr. Opin. Plant Biol. **8**:518–525.

Fitzpatrick, T.B. (2011). Vitamin B6 in plants: more than meets the eye. Adv. Bot. Res. **59**:1–38.

Fitzpatrick, T.B., Amrhein, N., Kappes, B., Macheroux, P., Tews, I., and Raschle, T. (2007). Two independent routes of de novo vitamin B6 biosynthesis: not that different after all. Biochem. J. **407**:1–13.

Gazzarrini, S., Lejay, L., Gojon, A., Ninnemann, O., Frommer, W.B., and von Wirén, N. (1999). Three functional transporters for constitutive, diurnally regulated, and starvation-induced uptake of ammonium into *Arabidopsis* roots. Plant Cell **11**:937–947.

Gjetting, K.S.K., Ytting, C.K., Schulz, A., and Fuglsang, A.T. (2012). Live imaging of intra- and extracellular pH in plants using pHusion, a novel genetically encoded biosensor. J. Exp. Bot. **63**:3207–3218.

Green, L.S., and Rogers, E.E. (2004). FRD3 controls iron localization in *Arabidopsis*. Plant Physiol. **136**:2523–2531.

Guan, M., de Bang, T.C., Pedersen, C., and Schjoerring, J.K. (2016). Cytosolic glutamine synthetase Gln1;2 is the main isozyme contributing to GS1 activity and can be up-regulated to relieve ammonium toxicity. Plant Physiol. **171**:1921–1933.

Hangarter, R.P., and Stasinopoulos, T.C. (1991). Effect of Fe-catalyzed photooxidation of EDTA on root-growth in plant culture media. Plant Physiol. **96**:843–847.

Havaux, M., Ksas, B., Szewczyk, A., Rumeau, D., Franck, F., Caffarri, S., and Triantaphylides, C. (2009). Vitamin B6 deficient plants display increased sensitivity to high light and photo-oxidative stress. BMC Plant Biol. **9**:130.

Ishiyama, K., Inoue, E., Watanabe-Takahashi, A., Obara, M., Yamaya, T., and Takahashi, H. (2004). Kinetic properties and ammonium-dependent regulation of cytosolic isoenzymes of glutamine synthetase in *Arabidopsis*. J. Biol. Chem. **279**:16598–16605.

Jain, S.K., and Lim, G. (2001). Pyridoxine and pyridoxamine inhibits superoxide radicals and prevents lipid peroxidation, protein glycosylation, and $(Na^+ + K^+)$-ATPase activity reduction in high glucose-treated human erythrocytes. Free Radic. Bio Med. **30**:232–237.

Jian, S.F., Liao, Q., Song, H.X., Liu, Q., Lepo, J.E., Guan, C.Y., Zhang, J.H., Ismail, A.M., and Zhang, Z.H. (2018). NRT1.1-related NH_4^+ toxicity is associated with a disturbed balance between NH_4^+ uptake and assimilation. Plant Physiol. **178**:1473–1488.

Jiang, C.F., Belfield, E.J., Mithani, A., Visscher, A., Ragoussis, J., Mott, R., Smith, J.A.C., and Harberd, N.P. (2012). ROS-mediated vascular homeostatic control of root-to-shoot soil Na delivery in *Arabidopsis*. EMBO J. **31**:4359–4370.

Ju, X.T., Xing, G.X., Chen, X.P., Zhang, S.L., Zhang, L.J., Liu, X.J., Cui, Z.L., Yin, B., Christie, P., Zhu, Z.L., et al. (2009). Reducing environmental risk by improving N management in intensive Chinese agricultural systems. Proc. Natl. Acad. Sci. U S A **106**:3041–3046.

Kannan, K., and Jain, S.K. (2004). Effect of vitamin B-6 on oxygen radicals, mitochondrial membrane potential, and lipid peroxidation in H_2O_2-treated U937 monocytes. Free Radic. Bio Med. **36**:423–428.

Kempinski, C.F., Haffar, R., and Barth, C. (2011). Toward the mechanism of NH_4^+ sensitivity mediated by *Arabidopsis* GDP-mannose pyrophosphorylase. Plant Cell Environ. **34**:847–858.

Khan, A.U., and Kasha, M. (1994). Singlet molecular-oxygen in the Haber-Weiss reaction. Proc. Natl. Acad. Sci. U S A **91**:12365–12367.

Konishi, N., Ishiyama, K., Beier, M.P., Inoue, E., Kanno, K., Yamaya, T., Takahashi, H., and Kojima, S. (2017). Contributions of two cytosolic glutamine synthetase isozymes to ammonium assimilation in *Arabidopsis* roots. J. Exp. Bot. **68**:613–625.

Lee, Y., Rubio, M.C., Alassimone, J., and Geldner, N. (2013). A mechanism for localized lignin deposition in the endodermis. Cell **153**:402–412.

Lešková, A., Zvari, K.M., Araya, T., and Giehl, R.F.H. (2020). Nickel toxicity targets cell wall-related processes and PIN2-mediated auxin transport to inhibit root elongation and gravitropic responses in *Arabidopsis*. Plant Cell Physiol. **61**:519–535.

Li, B.H., Li, G.J., Kronzucker, H.J., Baluska, F., and Shi, W.M. (2014). Ammonium stress in *Arabidopsis*: signaling, genetic loci, and physiological targets. Trends Plant Sci. **19**:107–114.

Li, G., Zhang, L., Wang, M., Di, D., Kronzucker, H.J., and Shi, W. (2019). The *Arabidopsis* AMOT1/EIN3 gene plays an important role in the amelioration of ammonium toxicity. J. Exp. Bot. **70**:1375–1388.

Li, Q., Li, B.H., Kronzucker, H.J., and Shi, W.M. (2010). Root growth inhibition by NH_4^+ in *Arabidopsis* is mediated by the root tip and is linked to NH_4^+ efflux and GMPase activity. Plant Cell Environ. **33**:1529–1542.

Li, X. (2011). Histostaining for tissue expression pattern of promoter-driven GUS activity in *Arabidopsis*. Bio **101**:e93.

Lima, J.E., Kojima, S., Takahashi, H., and von Wirén, N. (2010). Ammonium triggers lateral root branching in *Arabidopsis* in an AMMONIUM TRANSPORTER1;3-dependent manner. Plant Cell **22**:3621–3633.

Liu, Y., Lai, N., Gao, K., Chen, F., Yuan, L., and Mi, G. (2013). Ammonium inhibits primary root growth by reducing the length of meristem and elongation zone and decreasing elemental expansion rate in the root apex in *Arabidopsis thaliana*. PLoS ONE **8**:e61031.

Liu, Y., and von Wirén, N. (2017). Ammonium as a signal for physiological and morphological responses in plants. J. Exp. Bot. **68**:2581–2592.

Loqué, D., Ludewig, U., Yuan, L., and von Wirén, N. (2005). Tonoplast intrinsic proteins AtTIP2;1 and AtTIP2;3 facilitate NH_3 transport into the vacuole. Plant Physiol. **137**:671–680.

Lothier, J., Gaufichon, L., Sormani, R., Lemaitre, T., Azzopardi, M., Morin, H., Chardon, F., Reisdorf-Cren, M., Avice, J.C., and Masclaux-Daubresse, C. (2011). The cytosolic glutamine synthetase GLN1;2 plays a role in the control of plant growth and ammonium homeostasis in *Arabidopsis* rosettes when nitrate supply is not limiting. J. Exp. Bot. **62**:1375–1390.

Mahfouz, M.M., Zhou, S.Q., and Kummerow, F.A. (2009). Vitamin B6 compounds are capable of reducing the superoxide radical and lipid peroxide levels induced by H_2O_2 in vascular endothelial cells in culture. Int. J. Vitam. Nutr. Res. **79**:218–229.

Meier, M., Liu, Y., Lay-Pruitt, K.S., Takahashi, H., and von Wirén, N. (2020). Auxin-mediated root branching is determined by the form of available nitrogen. Nat. Plants **6**:1136–1145.

Moccand, C., Boycheva, S., Surriabre, P., Tambasco-Studart, M., Raschke, M., Kaufmann, M., and Fitzpatrick, T.B. (2014). The

pseudoenzyme PDX1.2 boosts vitamin B-6 biosynthesis under heat and oxidative stress in *Arabidopsis*. J. Biol. Chem. **289**:8203–8216.

Mooney, S., and Hellmann, H. (2010). Vitamin B6: killing two birds with one stone? Phytochemistry **71**:495–501.

Mora-Macías, J., Ojeda-Rivera, J.O., Gutierrez-Alanis, D., Yong-Villalobos, L., Oropeza-Aburto, A., Raya-Gonzalez, J., Jimenez-Dominguez, G., Chavez-Calvillo, G., Rellan-Alvarez, R., and Herrera-Estrella, L. (2017). Malate-dependent Fe accumulation is a critical checkpoint in the root developmental response to low phosphate. Proc. Natl. Acad. Sci. U S A **114**:E3563–E3572.

Müller, J., Toev, T., Heisters, M., Teller, J., Moore, K.L., Hause, G., Dinesh, D.C., Burstenbinder, K., and Abel, S. (2015). Iron-dependent callose deposition adjusts root meristem maintenance to phosphate availability. Dev. Cell **33**:216–230.

Nakayama, S., Sugano, S.S., Hirokawa, H., Mori, I.C., Daimon, H., Kimura, S., and Fukao, Y. (2020). Manganese treatment alleviates zinc deficiency symptoms in *Arabidopsis* seedlings. Plant Cell Physiol. **61**:1711–1723.

Nkebiwe, P.M., Weinmann, M., Bar-Tal, A., and Muller, T. (2016). Fertilizer placement to improve crop nutrient acquisition and yield: a review and meta-analysis. Field Crop Res. **196**:389–401.

Patterson, K., Cakmak, T., Cooper, A., Lager, I., Rasmusson, A.G., and Escobar, M.A. (2010). Distinct signalling pathways and transcriptome response signatures differentiate ammonium- and nitrate-supplied plants. Plant Cell Environ. **33**:1486–1501.

Percudani, R., and Peracchi, A. (2003). A genomic overview of pyridoxal-phosphate-dependent enzymes. EMBO Rep. **4**:850–854.

Qin, C., Qian, W.Q., Wang, W.F., Wu, Y., Yu, C.M., Jiang, X.H., Wang, D.W., and Wu, P. (2008). GDP-mannose pyrophosphorylase is a genetic determinant of ammonium sensitivity in *Arabidopsis thaliana*. Proc. Natl. Acad. Sci. U S A **105**:18308–18313.

Ragel, P., Rodenas, R., Garcia-Martin, E., Andres, Z., Villalta, I., Nieves-Cordones, M., Rivero, R.M., Martinez, V., Pardo, J.M., Quintero, F.J., et al. (2015). The CBL-interacting protein kinase CIPK23 regulates HAK5-mediated high-affinity K^+ uptake in *Arabidopsis* roots. Plant Physiol. **169**:2863–2873.

Raschke, M., Boycheva, S., Crevecoeur, M., Nunes-Nesi, A., Witt, S., Fernie, A.R., Amrhein, N., and Fitzpatrick, T.B. (2011). Enhanced levels of vitamin B-6 increase aerial organ size and positively affect stress tolerance in *Arabidopsis*. Plant J. **66**:414–432.

Raschle, T., Arigoni, D., Brunisholz, R., Rechsteiner, H., Amrhein, N., and Fitzpatrick, T.B. (2007). Reaction mechanism of pyridoxal 5′-phosphate synthase—detection of an enzyme-bound chromophoric intermediate. J. Biol. Chem. **282**:6098–6105.

Ristova, D., Carre, C., Pervent, M., Medici, A., Kim, G.J., Scalia, D., Ruffel, S., Birnbaum, K.D., Lacombe, B., Busch, W., et al. (2016). Combinatorial interaction network of transcriptomic and phenotypic responses to nitrogen and hormones in the *Arabidopsis thaliana* root. Sci. Signal. **9**:rs13.

Rogato, A., D'Apuzzo, E., Barbulova, A., Omrane, S., Parlati, A., Carfagna, S., Costa, A., Lo Schiavo, F., Esposito, S., and Chiurazzi, M. (2010). Characterization of a developmental root response caused by external ammonium supply in *Lotus japonicus*. Plant Physiol. **154**:784–795.

Romheld, V., and Marschner, H. (1986). Evidence for a specific uptake system for iron phytosiderophores in roots of grasses. Plant Physiol. **80**:175–180.

Roschzttardtz, H., Conejero, G., Curie, C., and Mari, S. (2009). Identification of the endodermal vacuole as the iron storage compartment in the *Arabidopsis* embryo. Plant Physiol. **151**:1329–1338.

Sanchez-Barrena, M.J., Chaves-Sanjuan, A., Raddatz, N., Mendoza, I., Cortes, A., Gago, F., Gonzalez-Rubio, J.M., Benavente, J.L., Quintero, F.J., Pardo, J.M., et al. (2020). Recognition and activation of the plant AKT1 potassium channel by the kinase CIPK23. Plant Physiol. **182**:2143–2153.

Shi, S.J., Xu, F.Z., Ge, Y.Q., Mao, J.J., An, L.L., Deng, S.J., Ullah, Z., Yuan, X.F., Liu, G.S., Liu, H.B., et al. (2020). NH_4^+ toxicity, which is mainly determined by the high NH_4^+/K^+ ratio, is alleviated by CIPK23 in *Arabidopsis*. Plants **9**:501.

Smirnoff, N., and Arnaud, D. (2018). Hydrogen peroxide metabolism and functions in plants. New Phytol. **221**:1197–1214.

Stolz, J., and Vielreicher, M. (2003). Tpn1p, the plasma membrane vitamin B_6 transporter of *Saccharomyces cerevisiae*. J. Biol. Chem. **278**:18990–18996.

Straub, T., Ludewig, U., and Neuhaeuser, B. (2017). The kinase CIPK23 inhibits ammonium transport in *Arabidopsis thaliana*. Plant Cell **29**:409–422.

Sun, L., Di, D.W., Li, G.J., Kronzucker, H.J., Wu, X.Y., and Shi, W.M. (2020). Endogenous ABA alleviates rice ammonium toxicity by reducing ROS and free ammonium via regulation of the SAPK9-bZIP20 pathway. J. Exp. Bot. **71**:4562–4577.

Sutton, M.A., Oenema, O., Erisman, J.W., Leip, A., van Grinsven, H., and Winiwarter, W. (2011). Too much of a good thing. Nature **472**:159–161.

Szydlowski, N., Burkle, L., Pourcel, L., Moulin, M., Stolz, J., and Fitzpatrick, T.B. (2013). Recycling of pyridoxine (vitamin B_6) by PUP1 in *Arabidopsis*. Plant J. **75**:40–52.

Tambasco-Studart, M., Titiz, O., Raschle, T., Forster, G., Amrhein, N., and Fitzpatrick, T.B. (2005). Vitamin B6 biosynthesis in higher plants. Proc. Natl. Acad. Sci. U S A **102**:13687–13692.

Thordal-Christensen, H., Zhang, Z.G., Wei, Y.D., and Collinge, D.B. (1997). Subcellular localization of H_2O_2 in plants. H_2O_2 accumulation in papillae and hypersensitive response during the barley-powdery mildew interaction. Plant J. **11**:1187–1194.

Tian, Q., Uhlir, N.J., and Reed, J.W. (2002). *Arabidopsis* SHY2/IAA3 inhibits auxin-regulated gene expression. Plant Cell **14**:301–319.

Titiz, O., Tambasco-Studart, M., Warzych, E., Apel, K., Amrhein, N., Laloi, C., and Fitzpatrick, T.B. (2006). PDX1 is essential for vitamin B6 biosynthesis, development and stress tolerance in *Arabidopsis*. Plant J. **48**:933–946.

Tsukagoshi, H. (2016). Control of root growth and development by reactive oxygen species. Curr. Opin. Plant Biol. **29**:57–63.

Tsukagoshi, H., Busch, W., and Benfey, P.N. (2010). Transcriptional regulation of ROS controls transition from proliferation to differentiation in the root. Cell **143**:606–616.

Vandesompele, J., De Preter, K., Pattyn, F., Poppe, B., Van Roy, N., De Paepe, A., and Speleman, F. (2002). Accurate normalization of real-time quantitative RT-PCR data by geometric averaging of multiple internal control genes. Genome Biol. **3**. https://doi.org/10.1186/gb-2002-3-7-research0034.

Wagner, S., Bernhardt, A., Leuendorf, J.E., Drewke, C., Lytovchenko, A., Mujahed, N., Gurgui, C., Frommer, W.B., Leistner, E., Fernie, A.R., et al. (2006). Analysis of the *Arabidopsis* rsr4-1/pdx1-3 mutant reveals the critical function of the PDX1 protein family in metabolism, development, and vitamin B6 biosynthesis. Plant Cell **18**:1722–1735.

Wasil, M., Halliwell, B., Grootveld, M., Moorhouse, C.P., Hutchison, D.C., and Baum, H. (1987). The specificity of thiourea, dimethylthiourea and dimethyl sulphoxide as scavengers of hydroxyl radicals. Their protection of alpha 1-antiproteinase against inactivation by hypochlorous acid. Biochem. J. **243**:867–870.

Watt, M., Silk, W.K., and Passioura, J.B. (2006). Rates of root and organism growth, soil conditions, and temporal and spatial development of the rhizosphere. Ann. Bot. **97**:839–855.

Xie, Y.J., Mao, Y., Xu, S., Zhou, H., Duan, X.L., Cui, W.T., Zhang, J., and Xu, G.H. (2015). Heme-heme oxygenase 1 system is involved in ammonium tolerance by regulating antioxidant defence in *Oryza sativa*. Plant Cell Environ. **38**:129–143.

Xu, G.H., Fan, X.R., and Miller, A.J. (2012). Plant nitrogen assimilation and use efficiency. Annu. Rev. Plant Biol. **63**:153–182.

Zheng, Z., Wang, Z., Wang, X.Y., and Liu, D. (2019). Blue light-triggered chemical reactions underlie phosphate deficiency-induced inhibition of root elongation of *Arabidopsis* seedlings grown in Petri dishes. Mol. Plant **12**:1515–1523.

Zhu, C.Q., Zhang, J.H., Zhu, L.F., Abliz, B., Zhong, C., Bai, Z.G., Hu, W.J., Sajid, H., James, A.B., Cao, X.C., et al. (2018). NH_4^+ facilitates iron reutilization in the cell walls of rice (*Oryza sativa*) roots under iron-deficiency conditions. Environ. Exp. Bot. **151**:21–31.